

Model-Free Assessment of Simulator Fidelity via Quantile Curves

Garud Iyengar* Yu-Shiou Willy Lin* Kaizheng Wang*

Abstract

As generative AI models are increasingly used to simulate real-world systems, quantifying the “sim-to-real” gap is critical. For each input setting of interest—which we call a *scenario*, such as a survey question or operating condition—the real and simulated systems are associated with unobserved latent population parameters, and their discrepancy varies across scenarios. A fundamental challenge is that, for any given scenario, this discrepancy cannot be observed directly, since both systems are accessible only through finite samples, often of heterogeneous sizes across scenarios. Standard predictive inference methods are therefore ill-suited, as they quantify uncertainty in observable outputs rather than latent population parameters. To address this, we construct confidence sets for these latent parameters and use them to derive a robust proxy for the sim-to-real discrepancy. We then estimate the quantile function of this proxy to obtain a distribution-level risk profile of the simulator, which supports a broad range of statistical summaries, including statistical inference for the real output distribution in a new scenario, the calculation of risk measures like Conditional Value-at-Risk (CVaR), and principled comparisons across simulators. Our method is model-agnostic and handles general output spaces, such as categorical survey responses and continuous multi-dimensional data. We demonstrate the practical utility of this method by evaluating the alignment of four major LLMs with human populations on the WorldValueBench dataset.

Keywords: Simulation, Quantile function estimation, Human-AI alignment, Conformal inference, Output Uncertainty Quantification

*Department of IEOR and Data Science Institute, Columbia University. Emails: garud@ieor.columbia.edu, y15782@columbia.edu, kaizheng.wang@columbia.edu.

1 Introduction

The adoption of simulators across operations and manufacturing, agent-based modeling in social-science research, user surveys, and education (Zhang et al., 2019; Macal, 2016; Argyle et al., 2023; Aher et al., 2023) has accelerated with recent advances in artificial intelligence (AI). At the platform level, industry ecosystems such as NVIDIA Omniverse and Earth-2 exemplify the push toward high-fidelity, AI-enabled digital twins, and LLMs are increasingly used to build generative agents that emulate human responses (Park et al., 2023; Lu et al., 2025). Collectively, these developments are driving growth in simulation across domains.

Against this backdrop, quantifying the *distributional* discrepancy between simulated and real-world outcomes is critical. This “sim-to-real” gap is a pervasive challenge in domains ranging from LLMs to computing systems and robotics (Gao et al., 2025; Durmus et al., 2023; Tobin et al., 2017; Peng et al., 2018). Crucially, it depends on the *scenario* (e.g., operating conditions or user prompts). In our setting, each scenario is associated with an unobserved *latent population quantity* for both the real system and the simulator, observed only through finite samples. As a simulator is deployed over a heterogeneous population of scenarios, the discrepancy between these latent scenario-level quantities becomes a random variable induced by the scenario distribution. Assessing fidelity therefore requires characterizing this discrepancy distribution, rather than a single average error, which can hide rare but consequential failures. This distributional characterization is the primary objective of our work.

Existing uncertainty quantification methods that focus on *individual* outcomes (e.g., conformal prediction) are insufficient for this task, as they do not gauge how well the simulator captures the true output distribution. Conflating outcome validity with distributional fidelity can have serious downstream implications. For instance, in survey research, an LLM-based simulator might generate coherent individual responses while yielding systematically biased *population-level aggregates* (Westwood, 2025). Recent work has identified distributional alignment as a key objective (Cao et al., 2025), and we address the practical challenge of assessment. We provide theoretical guarantees for sim-to-real discrepancy quantification without making structural assumptions about the simulator, treating it strictly as a black box.

Contributions We characterize the quantile function of the discrepancy between real and simulated output distributions across scenarios. Because the real-world distribution is only observed through finite, often heterogeneous, batches, the oracle quantile function is not directly computable. We construct per-scenario confidence sets for the latent real-world parameters, use them to form a proxy for the sim-to-real discrepancy, and establish finite-sample guarantees for the resulting quantile curve at any desired level. Moreover, we allow the coverage of the confidence-set to be chosen as a function of the number of sample available. This yields an adaptive procedure that produces tighter quantile curves in data-rich scenarios, while preserving reliability and interpretability when data are scarce.

We illustrate the methodology on *WorldValueBench* (Zhao et al., 2024), constructed from the World Values Survey (Haerpfer et al., 2020), by generating synthetic response profiles and benchmarking four LLMs against human survey data. Leveraging the large human sample size, we also study tightness and propose a data-driven procedure to construct confidence bands for the population quantile function.

Our main contributions are:

- (i) **Model-free, finite-sample fidelity profiling.** A black-box assessment framework with finite-sample, distributional guarantees under heterogeneous batching.
- (ii) **Quantile-based risk summaries.** A calibrated discrepancy quantile curve enabling the estimation of tail-risk measures, such as CVaR, and other summaries.

- (iii) **Inference and comparison.** Statistical inference for real-world parameters in new scenarios and principled comparisons across simulators.

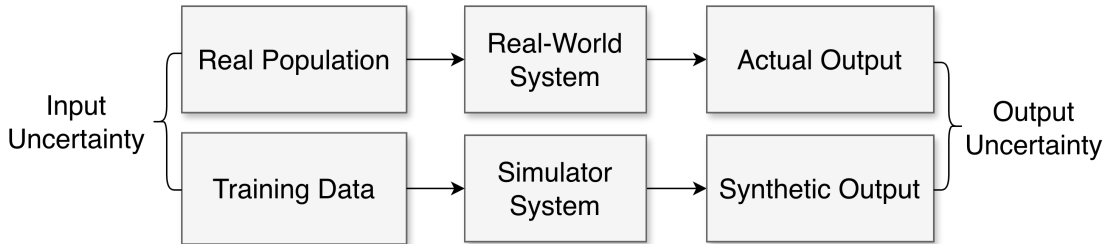


Figure 1: Simulation Uncertainty Quantification.

Related Literature The sim-to-real discrepancy has been the focus of the uncertainty quantification (UQ) literature. Figure 1 positions our work within this landscape. Following the taxonomy of Roy and Oberkamp (2011), we distinguish *input* uncertainty from *output* uncertainty. Work on input uncertainty (see Chen et al., 2024; Barton et al., 2014; Lam, 2022) typically assumes that the simulator model is known and it produces a faithful representation of the real world when the input follows the correct distribution. The goal is then to characterize how errors in characterizing the input distribution, due to a finite amount of noisy data, propagate to errors in the output. While early work on input uncertainty focused on confidence intervals at a fixed significance level α for functionals of the output, recent work by Chen et al. (2024) constructs Kolmogorov–Smirnov–type uncertainty bands for the CDF of the output discrepancy.

In contrast, modern digital twins rely on complex ML models (e.g., an LLM or a deep neural network), and one often does not have access to the model directly. Moreover, it can be computationally prohibitive to calibrate its parameters exactly. Consequently, we treat the simulator as a black box and focus on directly characterizing the sim-to-real discrepancy of the output—an approach termed *output uncertainty quantification* by Jeon et al. (2024). This perspective is related to simulation-based inference (SBI) (Cranmer et al., 2020; Papamakarios et al., 2019), which likewise studies inference with complex simulators, often under implicit generative models. The key difference is that SBI typically targets posterior inference on latent simulator parameters, whereas our goal is to assess the *output-level fidelity* of a fixed simulator across scenarios. Returning to the broader UQ literature, another distinction is that much of the work is asymptotic, whereas we provide finite-sample guarantees, which is critical when only a limited number of scenarios are available. Finally, while the classical input uncertainty literature is primarily concerned with Monte Carlo noise, which is the variance induced by stochastic sampling conditional on a fixed input model, our work incorporates both variance and bias of the simulator relative to the real world. This is precisely the focus of “sim-to-real” discrepancy.

Recent work in the LLM literature has also begun to study output uncertainty using model-agnostic discrepancy measures. For example, Santurkar et al. (2023a) aggregate the sim-to-real gap into a single scalar summary of overall error or bias, and Huang et al. (2025) bound the discrepancy at a fixed quantile level. These approaches correspond to evaluating particular functionals of the distribution of the sim-to-real discrepancy. More generally, the literature has largely emphasized scalar summaries or fixed-level bounds, leaving open the question of how to obtain a calibrated, distribution-level risk profile across scenarios. Two-sample testing is another nearby line of work. Kernel and related two-sample tests (Gretton et al., 2012; Schrab et al., 2023) are similarly sample-

based and often model-agnostic, but their primary goal is to determine whether two samples are distinguishable or consistent with having been drawn from the same distribution. By contrast, our target is not a global equality test between pooled real and simulated data, but the calibrated quantile profile of *scenario-level* sim-to-real discrepancy across scenarios.

To obtain such distribution-level guarantees in a model-agnostic way, we draw on ideas similar to conformal and predictive inference methods (Vovk et al., 2005; Bates et al., 2021), which provide finite-sample, distribution-free guarantees for black-box predictors. However, standard conformal formulations are typically stated in terms of *observable* outcomes (e.g., a future label or response) given each input, whereas our target is a *scenario-level distributional parameter* (e.g., the whole conditional output distribution or its functionals) that is only observed through finite batches, often of heterogeneous sizes. Recent conformal variants that target distributional objects (Snell et al., 2022; Budde et al., 2025) still assume homogeneous data, and do not directly address heterogeneous batching with latent scenario-level targets. We address this setting by providing finite-sample guarantees for quantile-based risk profiles of sim-to-real discrepancy when both real and simulated distributions are observed through heterogeneous batches.

The remainder of the paper proceeds as follows. In Section 2 we present a motivating example, and formally state the problem. In Section 3 we present the main theoretical results, and in Section 4 we discuss an application of our methodology. We also address the tightness of our methodology to the actual quantile curve in Section 5. In Section 6 we conclude by discussing future directions.

2 Framework and Motivating Example

We begin with a motivating use case through a survey-style LLM and then formalize the quantile estimation problem. Although we introduce the notation through an LLM example, the framework itself is more general. In Appendix D, we illustrate how the same formulation applies to other settings, including discrete-event manufacturing and broader control/scientific simulators with categorical and continuous outputs. Specifically, we ran our main numerical analysis under a survey setting, but conducted additional analysis in Appendix E under Building control setting in Appendix D.

Suppose a media research company plans to survey customers on a particular topic with multinomial outcomes (e.g., ‘Agree’, ‘Neutral’, ‘Disagree’). The company wants to estimate customer opinion before committing resources to an expensive population study. The company is considering whether to directly use a digital twin based on pre-trained LLM or to develop its own fine-tuned LLM. In order to make this decision, the company needs to evaluate the distribution of the sim-to-real gap across the range of questions that it is likely to encounter. While pre-trained LLMs can appear to provide coherent predictions, in Appendix E we show an example where several pre-trained LLMs underperform the baseline that randomly picks answers! The methods developed in this work can help with such assessments.

We formalize this setting and the associated theoretical challenges, by considering two sources of uncertainty: variation across scenarios and sampling noise within each scenario. First, we assume that scenarios (questions) are drawn from a population distribution, i.e. $\psi \sim \Psi$, and the past dataset consists of m scenarios $\{\psi_j\}_{j=1}^m$ drawn i.i.d. from Ψ . The real system (human) is characterized by a latent profile $z \in \mathcal{Z}$ distributed according to \mathcal{P} over \mathcal{Z} . For each pair (ψ, z) , the real system (human) produces a categorical outcome $Y^{\text{gt}} \in \{e_1, \dots, e_d\} \subset \mathbb{R}^d$, with conditional distribution $Q^{\text{gt}}(\cdot \mid z, \psi)$. The simulator (LLM) produces an outcome Y^{sim} with conditional distribution $Q^{\text{sim}}(\cdot \mid z^{\text{sim}}, \psi, r)$ over the same outcome space, where the $z^{\text{sim}} \in \mathcal{Z}_{\text{sim}}$ denotes a synthetic profile drawn i.i.d. from a simulator population distribution \mathcal{P}^{sim} on \mathcal{Z}_{sim} , and r denotes LLM settings,

including prompting strategy, hyperparameters, and other API settings.¹ In the running example, $Q^{\text{gt}}(\cdot | z, \psi) = \text{Categorical}(\Pi^{\text{gt}}(z, \psi))$, where $\Pi^{\text{gt}}(\psi, z) := (Q^{\text{gt}}(\{1\} | z, \psi), \dots, Q^{\text{gt}}(\{d\} | z, \psi)) \in \mathcal{P}^d$ and \mathcal{P}^d is the $d - 1$ -simplex $\{u \in [0, 1]^d : \sum_{i=1}^d u_i = 1\}$. For any question ψ , we can marginalize the population effect, hence denote by $Q^{\text{gt}}(\cdot | \psi) = \mathbb{E}_{z \sim \mathcal{P}}[Q^{\text{gt}}(\cdot | z, \psi)]$, the conditional distribution of outcome Y^{gt} given ψ .

Let $p(\psi)$ be a population statistic of interest, which is a functional of the conditional distribution $Q^{\text{gt}}(\cdot | \psi)$ and lives in a parameter space Θ . In our running example, $\Theta = \mathcal{P}^d$, $p(\psi)$ is the mean response of survey respondents, and simulator statistic of interest $q(\psi)$ can be defined similarly under the simulator population \mathcal{P}^{sim} . Further examples of $p(\psi)$ are given in Section 3. To simplify notation, we will write $p(\psi)$ and $q(\psi)$ as p_ψ and q_ψ . Summing up:

$$\begin{aligned} p_\psi &:= p(\psi) := \mathbb{E}_{y \sim Q^{\text{gt}}}[y] = \mathbb{E}_{z \sim \mathcal{P}}[\Pi^{\text{gt}}(\psi, z)] \in \Theta, \\ q_\psi &:= q(\psi) := \mathbb{E}_{z \sim \mathcal{P}^{\text{sim}}}[\Pi^{\text{sim}}(\psi, z)] \in \Theta. \end{aligned}$$

Second, we only observe finite samples per scenario. For each $j \in [m]$, we are given n_j i.i.d. profiles $z_{j,1:n_j} \sim \mathcal{P}$, with which we observe n_j ground-truth outcomes $y_{j,i}^{\text{gt}} \sim Q^{\text{gt}}(\cdot | z_{j,i}, \psi_j)$. Comparably, we generate k simulator outcomes $y_{j,\ell}^{\text{sim}} \sim Q^{\text{sim}}(\cdot | z_{j,\ell}^{\text{sim}}, \psi_j, r)$ using a simulation pool $z_{j,1:k}^{\text{sim}} \sim \mathcal{P}^{\text{sim}}$ with fixed k across j to standardize simulator sampling. For brevity, we will write to be \hat{p}_j and \hat{q}_j be plug-in estimators of p_j and q_j . In the motivating example these are empirical averages, though the formulation extends to more general plug-in estimators (e.g., empirical distributions or other scenario-level functionals).

Table 1: Illustrative Example of \mathcal{D}

Scenario	True Distribution (p_j)	n_j	Real Output (y^{gt})
1	(0.8, 0.1, 0.1)	10	(1, 1, 2, 3, 1, 2, 1, 1, 1, 1)
2	(0.3, 0.4, 0.3)	4	(3, 1, 2, 2)
\vdots	\dots	\vdots	\dots
m	(0.05, 0.05, 0.9)	8	(1, 3, 3, 3, 3, 2, 2, 3)

The dataset is $\mathcal{D} = \{(\psi_j, \hat{p}_j, \hat{q}_j, n_j, k)\}_{j=1}^m$. For each scenario j , let $\mathcal{D}_j^{\text{gt}} = \{(z_{ji}, y_{ji}^{\text{gt}})\}_{i=1}^{n_j}$ denote the human-side data used to construct \hat{p}_j , and $\mathcal{D}_j^{\text{sim}} = \{(z_{j\ell}^{\text{sim}}, y_{j\ell}^{\text{sim}})\}_{\ell=1}^k$ denote the simulator outputs used to construct \hat{q}_j . For concreteness, Table 1 provides an illustrative example of \mathcal{D} . Aligning with our motivating survey example, p_j is a multinomial parameter and the human sample sizes $\{n_j\}$ may vary across scenarios, so the realized outcomes $\{y_{ji}^{\text{gt}}\}$ differ both in content and in length. We record outcomes as category indices in $[d]$; equivalently, one may use one-hot encoding $e_y \in \mathbb{R}^d$. For instance, when $j = 2$ the true distribution is $p_2 = (0.3, 0.4, 0.3)$ and a sample of size $n_2 = 4$ yields $\hat{p}_2 = (0.25, 0.5, 0.25)$.

The discrepancy for a specific question ψ between simulated and real output distributions is defined as

$$\Delta_\psi := L(p_\psi, \hat{q}_\psi),$$

where $L : \Theta \times \Theta \rightarrow [0, \infty)$ is a user-chosen discrepancy function. We define the discrepancy in terms of \hat{q}_ψ to reflect a fixed simulator query budget; when simulator sampling is effectively unlimited,

¹We keep r fixed during calibration so that variation in \hat{q}_j reflects scenario differences rather than encoding drift or model choice; choosing a different r defines a different simulator.

one may replace \hat{q}_ψ with q_ψ to study the intrinsic discrepancy $L(p_\psi, q_\psi)$. We discuss this further in Section 3. Our method also works with any function L and allows practitioners to choose one that suits their application, e.g. Kullback–Leibler (KL) divergence for categorical outputs or a Wasserstein distance for nonparametric empirical distributions.

Now, we can state our task:

Construct a function $\hat{V}_m(\cdot, \mathcal{D}) : (0, 1) \rightarrow \mathbb{R}$ such that, for a new $\psi \sim \Psi$ and all $\tau \in (0, 1)$,

$$\mathbb{P}_{\psi \sim \Psi}(\Delta_\psi \leq \hat{V}_m(\tau, \mathcal{D}) | \mathcal{D}) \geq \tau - \varepsilon_m,$$

holds with high probability over the draw of \mathcal{D} and $\lim_{m \rightarrow \infty} \varepsilon_m = 0$.

Note that \hat{V}_m is indexed by both the prescribed level τ and the dataset \mathcal{D} . Establishing our desired result requires controlling two sources of uncertainty: (i) *scenario uncertainty*, since we observe only finitely many scenarios $\{\psi_j\}_{j=1}^m \sim \Psi$, and (ii) *finite-sample uncertainty* within each scenario, since p_j and q_j are only observed through finite samples that produce \hat{p}_j and \hat{q}_j . Our construction of $\hat{V}_m(\tau, \mathcal{D})$ explicitly accounts for both, and the main theorem will yield non-vacuous, finite-sample coverage guarantees.

We summarize the notations introduced in this section in Table 2, along with few upcoming notations from Section 3.

Table 2: Notation summary.

Symbol	Meaning
$\psi \sim \Psi$	Scenario drawn from the scenario population.
$z \sim P$	Real-world respondent drawn from the population distribution.
$p(\psi)$ (or p_ψ)	Real-world population parameter for scenario ψ .
$q(\psi)$ (or q_ψ)	Simulator-side population parameter for scenario ψ under fixed simulator settings.
$\hat{p}_\psi, \hat{q}_\psi$	Finite-sample estimators of p_ψ and q_ψ .
n_j	Human sample size for scenario j .
k (or k_j)	Simulator sample size for scenario j .
$L(\cdot, \cdot)$	Discrepancy function between real and simulated distribution.
Δ_ψ	True sim-to-real discrepancy for scenario ψ .
γ_j	Per-scenario confidence-set coverage level.
$\bar{\gamma}_m$	Average coverage level across m scenarios.
$\mathcal{C}_j(\hat{p}_j, \gamma_j)$	γ_j -confidence set for the latent parameter p_j .
$\hat{\Delta}_j$	Pseudo-discrepancy for scenario j , defined via a confidence set around \hat{p}_j .
$\hat{V}_m(\tau)$	Pseudo-discrepancy quantile curve built from m scenarios, indexed by quantile level τ .
τ	Quantile-function argument, counted in the usual direction from lower to upper quantiles.
α	Upper-tail fraction / exceedance level used when discussing tail scenarios.

3 Theoretical Result

In this section, we construct \hat{V}_m , establish its theoretical guarantees, and conclude by discussing the benefits of distribution-level fidelity guarantees.

3.1 Methodology

Our dataset \mathcal{D} consists of m scenarios; the true parameter value (resp. finite sample estimate) for scenario j is $p_j := p(\psi_j)$ (resp. \hat{p}_j); the simulator parameter value (resp. finite sample estimate) for

scenario j is $q_j := q(\psi_j)$ (resp. \hat{q}_j).

Our procedure has two steps:

1. For each j , define a γ_j -confidence set $\mathcal{C}_j(\hat{p}_j, \gamma_j)$, i.e.

$$\mathbb{P}(p_j \in \mathcal{C}_j(\hat{p}_j, \gamma_j)) \geq \gamma_j, \quad (3.1)$$

and the pseudo-discrepancy

$$\hat{\Delta}_j := \sup_{u \in \mathcal{C}_j(\hat{p}_j, \gamma_j)} L(u, \hat{q}_j). \quad (3.2)$$

2. For $\alpha \in (0, 1)$, let

$$\hat{V}_m(\tau) := \text{the } \tau\text{-quantile of } \{\hat{\Delta}_j\}_{j=1}^m. \quad (3.3)$$

We will show that $\hat{V}_m(\tau)$ is a calibrated quantile curve for the discrepancy distribution, up to explicit finite-sample corrections. Note that the key design choice in our method is the confidence set $\mathcal{C}_j(\cdot)$ that quantifies the uncertainty of \hat{p}_j . This uncertainty set is the key device that links per-scenario sampling error to distribution-level calibration. Next, we show how to construct these sets using off-the-shelf concentration bounds, starting with the multinomial setting.

Example 3.1 (Multinomial Confidence Set). *Suppose the outcomes are multinomial with parameter $p_j \in \Theta = \mathcal{P}^d := \{u \in [0, 1]^d : \sum_{i=1}^d u_i = 1\}$, i.e., $Y_{j,i} \mid \psi_j \sim \text{Categorical}(p_j)$ and \hat{p}_j is the empirical average vector from n_j samples. Let $\text{KL}(\cdot \parallel \cdot)$ denote the KL divergence. Then*

$$\mathcal{C}_j(\hat{p}_j, \gamma_j) := \left\{ u \in \mathcal{P}^d : \text{KL}(\hat{p}_j \parallel u) \leq \frac{d-1}{n_j} \ln \left(\frac{2(d-1)}{1-\gamma_j} \right) \right\}.$$

is a γ_j -confidence set for p_j .

This result is a variant of Chernoff-Hoeffding Bound, see Lemma A.5 (Mardia et al., 2019).

Example 3.2 (Bounded Outcomes). *Suppose $Y_{j,i} \in [a, b]$ are i.i.d. with population mean $p_j := \mathbb{E}[Y_{j,i}]$ for scenario j , and $\hat{p}_j := \frac{1}{n_j} \sum_{i=1}^{n_j} Y_{j,i}$ is the sample mean. Then*

$$\mathcal{C}_j(\hat{p}_j, \gamma_j) := \left\{ u \in [a, b] : |u - \hat{p}_j| \leq (b-a) \sqrt{\frac{\log(2/(1-\gamma_j))}{2n_j}} \right\},$$

is a γ_j -confidence set for p_j .

Example 3.3 (Nonparametric W_1 Confidence Set). *Suppose the true outcome distribution for scenario j is P_j and samples are drawn as $Y_{j,1:n_j} \stackrel{iid}{\sim} P_j$. Assume P_j is σ -sub-Gaussian. Let \hat{P}_j denote the empirical distribution from n_j samples. Then*

$$\mathcal{C}_j^{W_1}(\hat{P}_j, \gamma_j) := \left\{ Q : W_1(\hat{P}_j, Q) \leq r_j(n_j, \gamma_j, \sigma) \right\},$$

where

$$r_j = \frac{512\sigma}{\sqrt{n_j}} + \sigma \sqrt{\frac{256e}{n_j} \log \frac{1}{1-\gamma_j}},$$

is a γ_j -confidence set for the true distribution P_j .

The form of \mathcal{C}_j is justified by the concentration inequality proved in L.A. and Bhat (2022). Next, we show that $\hat{\Delta}_j$ can be efficiently computed for each scenario j .

- (a) *KL-Divergence*: For $\mathcal{C}_j(\hat{p}_j, \gamma_j) = \{u \in \mathcal{P}^d : \text{KL}(\hat{p}_j \| u) \leq r_j\}$ and loss $L(u, \hat{q}_j) = \text{KL}(u \| \hat{q}_j)$, the pseudo-discrepancy

$$\hat{\Delta}_j = \sup_{u \in \mathcal{C}_j(\hat{p}_j, \gamma_j)} \text{KL}(u \| \hat{q}_j).$$

The maximizer lies on the boundary $\text{KL}(\hat{p}_j \| u) = r_j$ and can be computed via standard maximization.

- (b) *Wasserstein-1*: For $\mathcal{C}_j^{W_1}(\hat{P}_j, \gamma_j) = \{u : W_1(u, \hat{P}_j) \leq r_j\}$ and loss $L(u, \hat{Q}_j) = W_1(u, \hat{Q}_j)$, triangle inequality implies that

$$\hat{\Delta}_j = \sup_{u \in \mathcal{C}_j^{W_1}(\hat{P}_j, \gamma_j)} W_1(u, \hat{Q}_j) \leq W_1(\hat{P}_j, \hat{Q}_j) + r_j.$$

3.2 Calibrated Quantile Curve Theory

Our theoretical guarantee relies on the following two assumptions.

Assumption 3.1 (Independent data). *The scenarios $\psi_j \sim \Psi$ are i.i.d., $\mathcal{D}_j^{\text{gt}} \perp\!\!\!\perp \mathcal{D}_j^{\text{sim}}$ conditioned on ψ_j , and the new $(\psi, \mathcal{D}^{\text{sim}})$ is independent of \mathcal{D} . In addition, the human sample sizes $\{n_j\}_{j=1}^m$ are treated as fixed (deterministic) design quantities.*

Assumption 3.2 (Regular Discrepancy). *The discrepancy $L : \Theta \times \Theta \rightarrow [0, \infty)$ is jointly continuous on $\Theta \times \Theta$ and satisfies $L(u, u) = 0$ for all $u \in \Theta$.*

Before stating our main result, we consider the special case $\gamma_j \equiv \frac{1}{2}$. Then, in the asymptotic regime $m \rightarrow \infty$, our guarantee (3.6) implies the following: for any target quantile level $\tau \in (0, 1)$,

$$\mathbb{P}_{\psi \sim \Psi} \left(\Delta_\psi \leq \hat{V}_m \left(\frac{1+\tau}{2} \right) \middle| \mathcal{D} \right) \geq \tau. \quad (3.4)$$

In words, the τ -quantile of the discrepancy Δ_ψ is approximated by the empirical pseudo-quantile curve at an *inflated index* $(1 + \tau)/2$. This inflation induces an inherent conservativeness: for $\tau \approx 0$, the index $(1 + \tau)/2$ is at least the median of the pseudo-discrepancy distribution, leading to substantial inflation in the lower tail.

In general, the γ_j 's can be different, and we obtain the following asymptotic result:

$$\mathbb{P}_{\psi \sim \Psi} \left(\Delta_\psi \leq \hat{V}_m (\bar{\gamma}_m \tau + (1 - \bar{\gamma}_m)) \middle| \mathcal{D} \right) \geq \tau, \quad (3.5)$$

where $\bar{\gamma}_m = \frac{1}{m} \sum_{j=1}^m \gamma_j$. Now, to achieve τ -level coverage we evaluate the empirical pseudo-quantile at an index that is affine in τ with slope $\bar{\gamma}_m$. One would ideally want $\bar{\gamma}_m = 1$, or equivalently $\gamma_j \equiv 1$, to control the index inflation. However, increasing γ_j typically enlarges the set \mathcal{C}_j , and thus, increases the values of the pseudo-discrepancies $\hat{\Delta}_j$ and shift the curve \hat{V}_m upward. Thus, one needs to balance index adjustment with increased conservativeness of the pseudo-quantile curve itself.

This trade-off motivates choosing γ_j adaptively as a function of the human sample size n_j . When n_j is large, p_j is typically more concentrated around \hat{p}_j ; therefore, γ_j can be set high without significantly enlarging \mathcal{C}_j . Therefore, we set $\gamma_j = g(n_j)$, for an increasing function $g : \mathbb{R}_+ \rightarrow [0, 1]$. See Section 4 for numerical evidence illustrating the conservativeness of fixed γ and the benefits of adaptive coverage. We are now ready to rigorously state the main theorem.

Theorem 3.1. *Suppose Assumptions 3.1–3.2 hold and $\gamma_j \in (0, 1)$ for each $j \in [m]$. Let $\mathcal{C}_j(\hat{p}_j, \gamma_j)$ denote any γ_j -confidence set (see (3.1)), $\hat{\Delta}_j$ denote the pseudo-discrepancy (see (3.2)), and let \hat{V}_m denote the quantile function of the pseudo-discrepancy (see (3.3)). For $\alpha \in (0, 1)$, let $[\alpha]_m := m^{-1} \lceil m\alpha \rceil$ denote the rounded empirical grid point associated with α , so that $[\alpha]_m \in [\alpha, \alpha + \frac{1}{m}]$, and let $[x]_+ := \max\{x, 0\}$. Set*

$$\alpha_{\text{eff}}(\alpha) := \left[(\bar{\gamma}_m - \varepsilon_{\text{al}}(\alpha, \delta)) [\alpha]_m - b_m(\delta) \sqrt{[\alpha]_m} \right]_+,$$

where $\bar{\gamma}_m := \frac{1}{m} \sum_{j=1}^m \gamma_j$, $\varepsilon_{\text{al}}(\alpha, \delta) = \sqrt{\frac{\log(3m/\delta)}{2m[\alpha]_m}}$, and $b_m(\delta) = \sqrt{\frac{1}{2m} \log \frac{3m}{\delta}}$. Then, with probability at least $1 - \delta$ over \mathcal{D} , simultaneously for all $\alpha \in (0, 1)$,

$$\mathbb{P}_{\psi \sim \Psi} \left(\Delta_{\psi}^{(k)} \leq \hat{V}_m(1 - \alpha_{\text{eff}}(\alpha)) \mid \mathcal{D} \right) \geq 1 - \alpha - \varepsilon_m(\delta), \quad (3.6)$$

where $\varepsilon_m(\delta) := \sqrt{\frac{\log(6/\delta)}{2m}} + \frac{1}{m}$. In particular, the remainder terms $\varepsilon_m, \varepsilon_{\text{al}}$, and $b_m \rightarrow 0$ as $m \rightarrow \infty$.

Unlike standard conformal inference, which targets uncertainty quantification for future observable outcomes (e.g. responses), Theorem 3.1 provides uncertainty quantification for the latent, scenario-specific population parameter that governs outcome generation (e.g. conditional mean response). In other words, the guarantee operates at the level of underlying distributions, in contrast to single draws. We next provide a proof sketch.

Proof Sketch:

Suppose we have access to the true p_j for each scenario j . Then $\{\Delta_j\}_{j=1}^m$ are i.i.d., and the Dvoretzky–Kiefer–Wolfowitz (DKW) inequality yields a uniform deviation bound for the empirical CDF of the discrepancy, which can be translated into upper bounds on its quantile function. In our setting, however, (i) p_j is latent and (ii) each scenario is observed with a heterogeneous sample size n_j .

Our goal is to use empirical quantiles of the observable proxy $\{\hat{\Delta}_j\}$ to approximate the quantile function of the unobservable discrepancies $\{\Delta_j\}$. For simplicity, we fix $\gamma_j \equiv \gamma$. The key steps are as follows:

- Let t_α denote the population $(1 - \alpha)$ -quantile of Δ_j , and define the corresponding hardest scenarios $S_\alpha := \{j : \Delta_j \geq t_\alpha\}$. By definition, $\frac{|S_\alpha|}{m} \approx \alpha$.
- By construction, $\hat{\Delta}_j \geq \Delta_j$ holds with probability γ for each j . Consequently, among indices in S_α , at least a γ -fraction satisfy $\hat{\Delta}_j \geq t_\alpha$.
- Hence, at least a $\gamma\alpha$ -fraction of the pseudo-discrepancies exceed t_α . In other words, the $(1 - \alpha)$ quantile of Δ_j is dominated by the $(1 - \gamma\alpha)$ quantile of $\hat{\Delta}_j$.

Therefore, for any quantile level $\tau := 1 - \alpha$, taking the $(\gamma\tau + (1 - \gamma))$ -quantile of the pseudo-discrepancies yields an upper bound on the τ -quantile of the oracle discrepancies.

This is why the quantile index must shift: to upper bound the oracle τ -quantile of Δ , we need to use a more conservative pseudo-quantile level so that the resulting pseudo-threshold is high enough to cover the target quantile despite the miscoverage. This index adjustment is the first source of conservativeness; the second source is the DKW deviation that relates empirical and population CDFs over finitely many scenarios. Combining these two ingredients yields the theorem. The complete proof is in Appendix B.1. \square

Remark 1. A subtle modeling choice is that Theorem 3.1 characterizes the distribution of $\Delta^{(k)} = L(p, \hat{q}^{(k)})$, where $\hat{q}^{(k)}$ is estimated using k simulator samples, instead of the actual simulator parameter q . Conceptually, $\Delta^{(k)}$ is the *correct* target when one wants to characterize performance for a fixed query budget k . In contrast, Δ is more natural when simulator queries are cheap, and the goal also includes quantifying the simulator’s inherent bias. For brevity, we will, henceforth, ignore the k superscript in following discussions. A proof to the latter case is presented in Corollary B.2, see Appendix B for details.

3.3 Benefits of Distribution-Level Characterization

We now turn to the benefits of obtaining a distributional-level characterization of sim-to-real discrepancy. For illustrative purposes we set $\bar{\gamma}_m = \frac{1}{2}$. With this calibrated quantile, for an unseen scenario ψ we can derive a confidence set for p_ψ given a simulated \hat{q}_ψ . For a target confidence level $\bar{\alpha} \in (0, 1)$, define

$$S_{\bar{\alpha}} := \{u \in \Theta : L(u, \hat{q}_\psi) \leq \tau_{\bar{\alpha}}\}, \quad \tau_{\bar{\alpha}} := \hat{V}_m(1 - \frac{\bar{\alpha}}{2}).$$

By Theorem 3.1, $p_\psi \in S_{\bar{\alpha}}$ with probability at least $1 - \bar{\alpha}$ up to an $o_m(1)$ remainder.

In addition, the calibrated quantile curve can be compressed to provide summary statistics, hence strictly more informative than any single risk summary. Returning to the motivating example, a media research firm can use a calibrated AUC to assess average simulator bias, while a pollster or risk-averse product team may track a calibrated CVaR $_\alpha$ to bound rare but consequential misreads of public sentiment.

Concretely, define the index-adjusted (calibrated) curve

$$\hat{V}_m^{\text{cal}}(\tau) := \hat{V}_m\left(\frac{1+\tau}{2}\right), \quad \tau \in [0, 1],$$

which matches the coverage guarantee in Equation 3.4 in asymptotic regime. We then summarize overall average sim-to-real discrepancy via the calibrated AUC

$$\text{AUC}_{\text{cal}} := \int_0^1 \hat{V}_m^{\text{cal}}(\tau) d\tau,$$

and tail risk via a calibrated right-tail CVaR: for $\alpha \in (0, 1)$,

$$\text{CVaR}_\alpha^{\text{cal}} := \frac{1}{\alpha} \int_{1-\alpha}^1 \hat{V}_m^{\text{cal}}(u) du.$$

In words, AUC_{cal} aggregates the entire calibrated curve into a single average-bias summary, while $\text{CVaR}_\alpha^{\text{cal}}$ averages over the worst α fraction of scenarios under the same index-adjusted quantile curve.

4 Application: LLM Fidelity Profiling

4.1 Dataset and Methodology

We evaluate our procedure on the *WorldValueBench* dataset, curated by Zhao et al. (2024) and constructed from the World Values Survey (Haerpfer et al., 2020). The dataset comprises survey questions asked across 64 countries, covering 12 thematic categories (e.g., social values, security, migration). Individual-level covariates are available for each respondent, including gender, age, migration status, education, marital status, and related demographics.

Q199. How interested would you say you are in politics? Are you

- 1 Very interested
- 2 Somewhat interested
- 3 Not very interested
- 4 Not at all interested

Figure 2: Example of World Value Question. Source: Haerpfer et al. (2020).

Preprocessing. After data cleaning, we retain 235 distinct questions and responses from 96,220 individuals. Each question offers a categorical set of possible answers, as illustrated in Figure 2. To place heterogeneous answer sets on a common scale, we map each question’s categories to the interval $[-1, 1]$, producing a bounded real-valued outcome for every scenario and respecting the natural ordering of response options when available (e.g., disagree–neutral–agree). Individual-level covariates are then used to construct synthetic profiles and corresponding prompts for simulators. Additional details on preprocessing and dataset characteristics are provided in Appendix C.

Methodology We generate synthetic responses and estimate $\{\hat{q}_j\}_{j=1}^{235}$ for four LLMs: GPT-4o (gpt-4o), GPT-5 MINI (gpt-5-mini), LLAMA 3.3 70B (Llama-3.3-70B-Instruct-Turbo), and QWEN 3 235B (Qwen3 235B A22B Thinking 2507 FP8). As a benchmark, we also construct a *uniform* baseline: for each question, this generator samples an answer uniformly at random from the available choices for each individual. We simulate 200 LLM samples per question, and use these simulated responses to estimate \hat{q}_j . For humans, we subsample 500 respondents per question to calculate $\{\hat{p}_j\}_{j=1}^{235}$ and construct the corresponding confidence sets \mathcal{C}_j . Due to nonresponses, the effective sample size n_j varies across questions (typically 450–500).

Since the outcome is bounded in $[-1, 1]$, we construct per-scenario confidence sets \mathcal{C}_j using Example 3.2. We set $\gamma_j = 1 - n_j^{-1/3}$, which is increasing in sample size n_j^2 , and yields an average coverage level of $\bar{\gamma}_m \approx 0.87$. The loss function $L(p, q) = (p - q)^2$. Next, we use the procedure described in Section 3 (see (3.1)-(3.3)) to obtain a fidelity profile for each candidate LLM, and plot the calibrated curve using the asymptotic index adjustment in (3.5). For completeness, we also apply the same workflow to a Bernoulli setting (EEDI), multinomial setting (OpinionQA) and a continuous temperature prediction setting (UMAR dataset from NEST); see Appendix E.

4.2 Fidelity Profiling

The calibrated quantile functions for the four different LLMs are plotted in Figure 3. Lower, flatter curves indicate uniformly small discrepancies, while elbows reveal rare but severe misses. Our results suggest that all LLM-simulators outperform the uniform benchmark on over 80% of questions, but fail to capture the tail scenarios. GPT-4O is the lowest across all quantiles, indicating the most reliable alignment, with GPT-5-MINI close behind yet failing to capture some outlier questions, and LLAMA 3.3 and QWEN-3 trail behind. While this comparison is useful, we want to emphasize that the uniform baseline is not intended to represent a universally poor simulator. For some near-balanced questions, it can return low sim-to-real gap. Its role here is instead to serve as a simple

²As discussed in Section 3, the coverage level $\gamma_j = g(n_j)$ should increase with the sample size n_j . We therefore adopt a generic form $\gamma_j = 1 - n_j^{-\beta}$, and conduct a sensitivity analysis on β value in Appendix C.4.

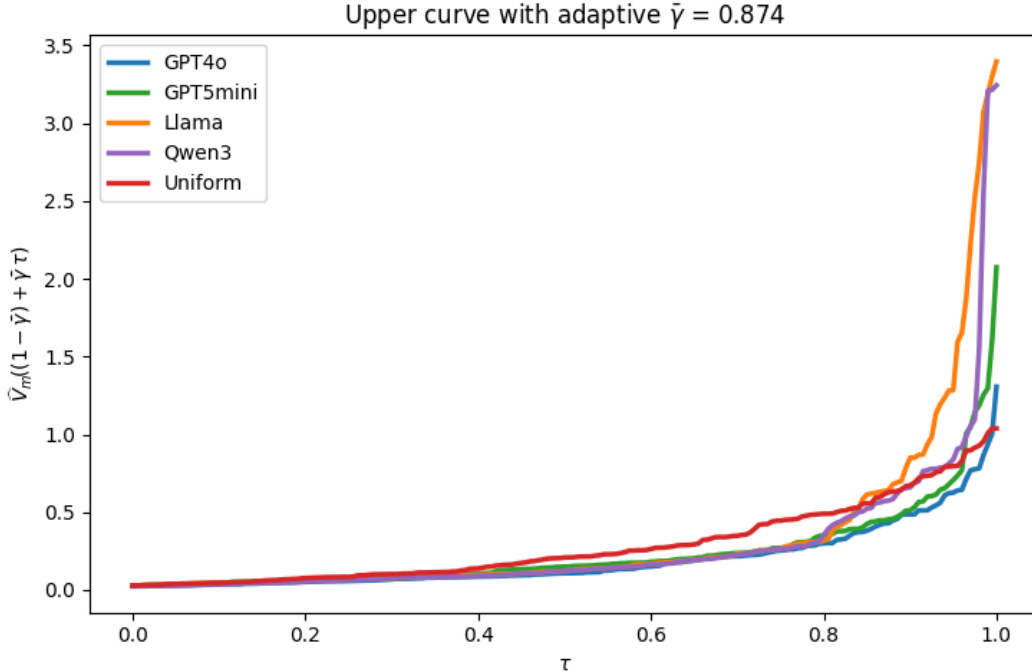


Figure 3: Calibrated discrepancy quantile curves $\hat{V}(\tau)$ across LLM simulators. Colors: **blue** = GPT-4o, **green** = GPT-5-MINI, **orange** = LLAMA 3.3, **purple** = QWEN-3, and **red** = the uniform baseline.

structure-free reference for illustrating how the proposed framework compares simulator fidelity at the scenario level.

We also provide a robustness check on whether the dominance relation is an anomaly of the particular choice for the sample size n_j . Figure 4 shows performance of the LLMs for $n_j = \{50, 500, 5000, 10000\}$. The results indicate that the dominance relation between LLMs remains the same.

5 Tightness Analysis of Calibrated Quantiles

A natural concern with our approach is the tightness of our calibrated quantile curve. Since our construction relies on off-the-shelf concentration bounds and worst-case pseudo-discrepancies, the resulting calibrated quantiles could, in principle, be conservative to the point of being vacuous. To assess this empirically, we conduct a tightness study in a setting that leverages a feature of WorldValueBench.

We leverage the WorldValueBench benchmark, which contains up to 96,220 respondents per question. We treat the empirical distribution \hat{p}_j computed from all available respondents as a proxy for the true human response distribution p_j . This enables computation of an “oracle” discrepancy $\Delta_j^* := L(p_j, \hat{q}_j)$, and hence an oracle quantile curve across questions. We fix the simulator budget at $k = 200$ and, for each question j , subsample $n_j \in \{50, 500, 1000, 5000\}$ respondents to construct the confidence sets and pseudo-discrepancies $\{\hat{\Delta}_j\}_{j=1}^m$. We then compare the resulting calibrated curves against the oracle quantile curve.

The results plotted in Figure 5 indicate that the calibrated envelope is substantially conservative when $n_j = 50$, but becomes tighter when $n_j \geq 500$. This behavior is consistent with our construction: larger n_j yields more concentrated estimates \hat{p}_j and smaller confidence sets $\mathcal{C}_j(\hat{p}_j, \gamma_j)$, which reduces

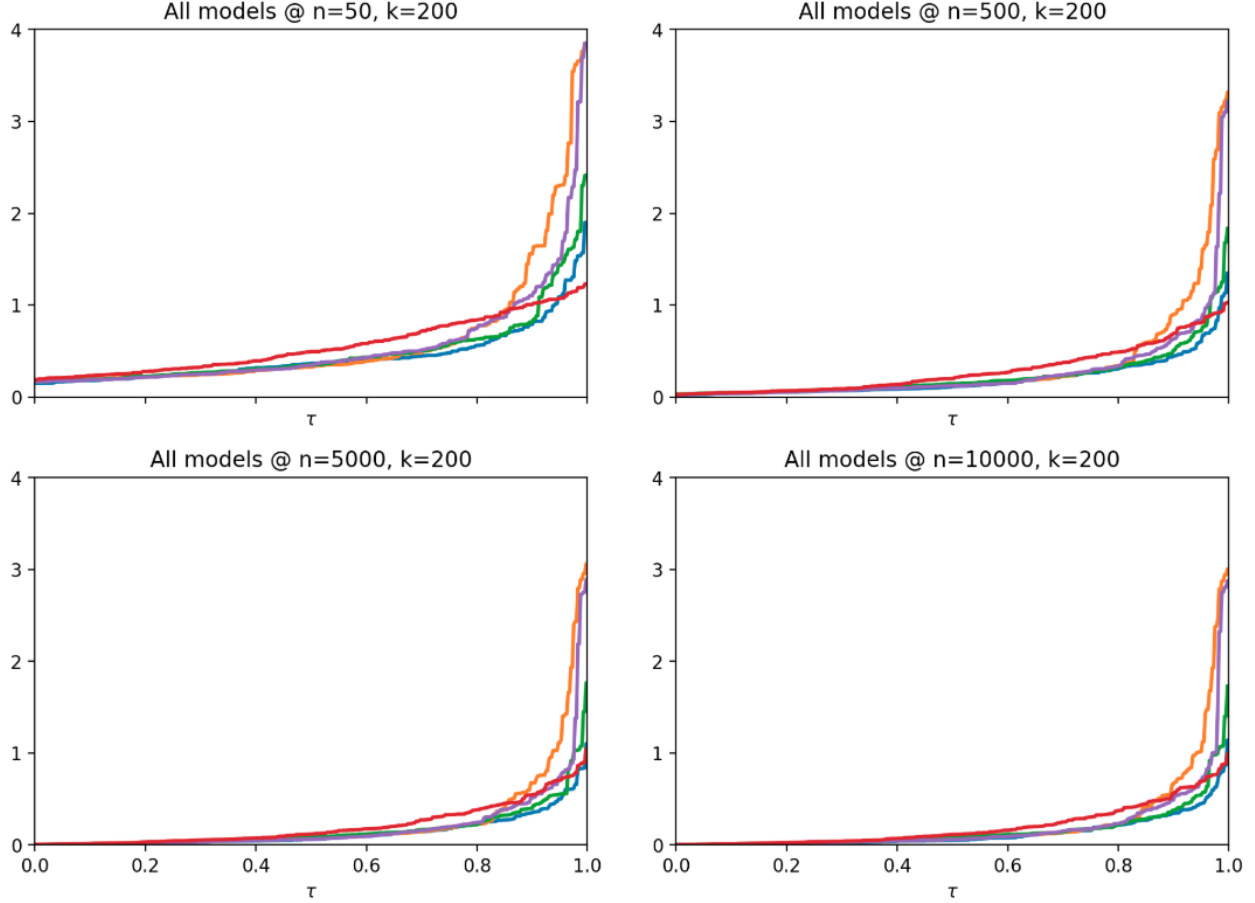


Figure 4: Robustness check of simulator performance under different human sample sizes. Panels correspond to $n_j = 50$ (top left), $n_j = 500$ (top right), $n_j = 5000$ (bottom left), and $n_j = 10000$ (bottom right), with $k = 200$ fixed. Colors match Figure 3.

the inflation induced by the supremum defining $\hat{\Delta}_j$.

The results in Figure 5 correspond to $\gamma_j = 1 - n_j^{-\frac{1}{3}}$. In order to isolate the impact of batch-size-specific γ_j , as we discussed in Section 3, we repeat the same experiment by setting $\gamma_j \equiv \frac{1}{2}$ for all questions. The corresponding results are plotted in Figure 6. The plots here exhibit a persistent vertical separation between the oracle quantile curve and the calibrated curves, even for large n_j . This phenomenon is explained by the fact that here $\bar{\gamma}_m = \frac{1}{2}$ (independent of n_j) and the asymptotic calibration evaluates the pseudo-quantile at $\hat{V}_m(0.5\tau + 0.5)$. Consequently, at lower quantile levels ($\tau \approx 0$), our procedure approximates the quantile function by at least the median, inducing a non-vanishing conservativeness that cannot be eliminated by increasing n_j . This underscores the importance of allowing scenario-dependent coverage levels.

While WorldValueBench provides a large pool of respondents that facilitates an oracle tightness check, most applications do not enjoy such extensive ground-truth data. We next develop a complementary tightness assessment: a confidence band that sandwiches the oracle quantile curve.

Theorem 5.1 (Informal Version). *Suppose the setup of Theorem 3.1 and Assumptions 3.1–3.2 hold.*

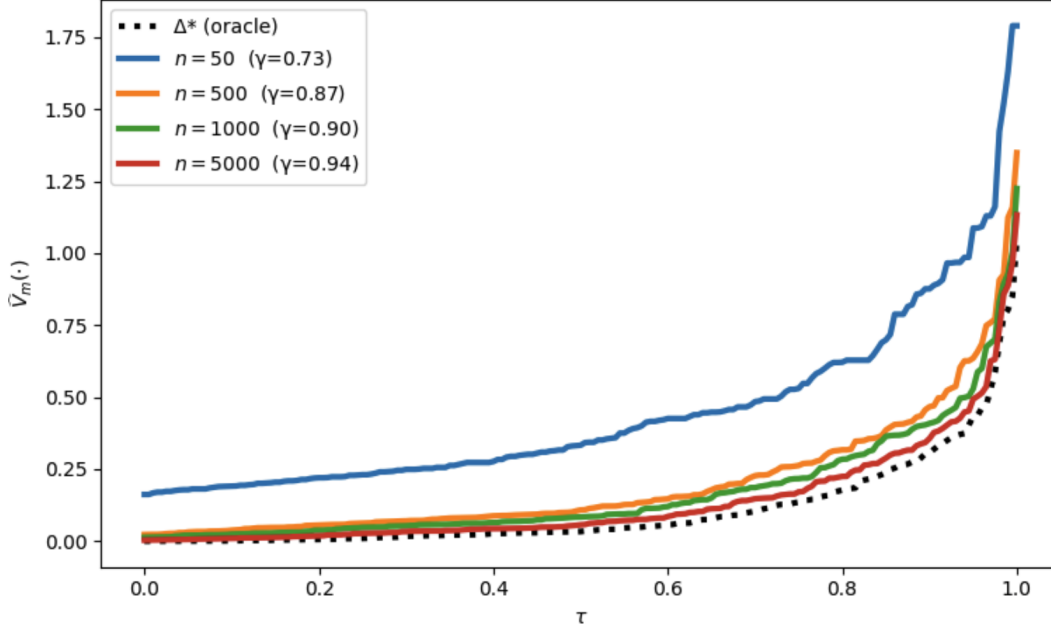


Figure 5: Tightness analysis for varying n_j under GPT-4o. The dotted black curve is the oracle quantile curve Δ^* ; the colored curves are calibrated curves computed from subsamples with $n_j = 50$ (blue), $n_j = 500$ (orange), $n_j = 1000$ (green), and $n_j = 5000$ (red). The corresponding adaptive average coverage levels shown in the legend are $\bar{\gamma} \approx 0.73, 0.87, 0.90$, and 0.94 , respectively.

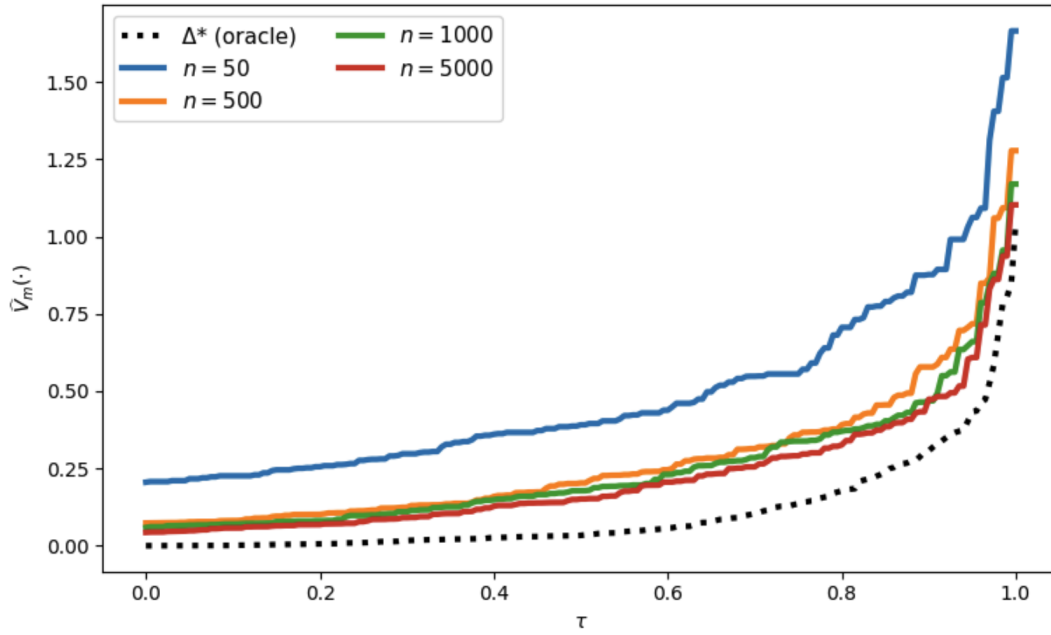


Figure 6: Tightness analysis for varying n_j under GPT-4o with fixed $\gamma_j = \frac{1}{2}$. Colors match Figure 5.

Let $\{\gamma_{L,j}, \gamma_{U,j}\}_{j=1}^m \subset (0, 1]$ be coverage levels and define the lower and upper pseudo-discrepancies

$$\hat{\Delta}_j^- := \inf_{u \in \mathcal{C}_j(\hat{p}_j, \gamma_{L,j})} L(u, \hat{q}_j), \quad \hat{\Delta}_j^+ := \sup_{u \in \mathcal{C}_j(\hat{p}_j, \gamma_{U,j})} L(u, \hat{q}_j),$$

where $\mathcal{C}_j(\hat{p}_j, \gamma) \subset \Theta$ are γ -confidence sets. Let $\hat{V}_m^-(\cdot)$ (resp. $\hat{V}_m^+(\alpha)$) denote the empirical quantile function of $\{\hat{\Delta}_j^-\}_{j=1}^m$ (resp. $\{\hat{\Delta}_j^+\}_{j=1}^m$). Let $V : [0, 1] \rightarrow \mathbb{R}$ denote the quantile function of $\Delta(\psi)$. Then, as $m \rightarrow \infty$, for any fixed $\tau \in (0, 1)$,

$$\hat{V}_m^-(\bar{\gamma}_{L,m}\tau) \lesssim V(\tau) \lesssim \hat{V}_m^+(\bar{\gamma}_{U,m}\tau + (1 - \bar{\gamma}_{U,m})), \quad (5.1)$$

where $\bar{\gamma}_{L,m} = \frac{1}{m} \sum_{j=1}^m \gamma_{L,j}$, and $\bar{\gamma}_{U,m} = \frac{1}{m} \sum_{j=1}^m \gamma_{U,j}$.

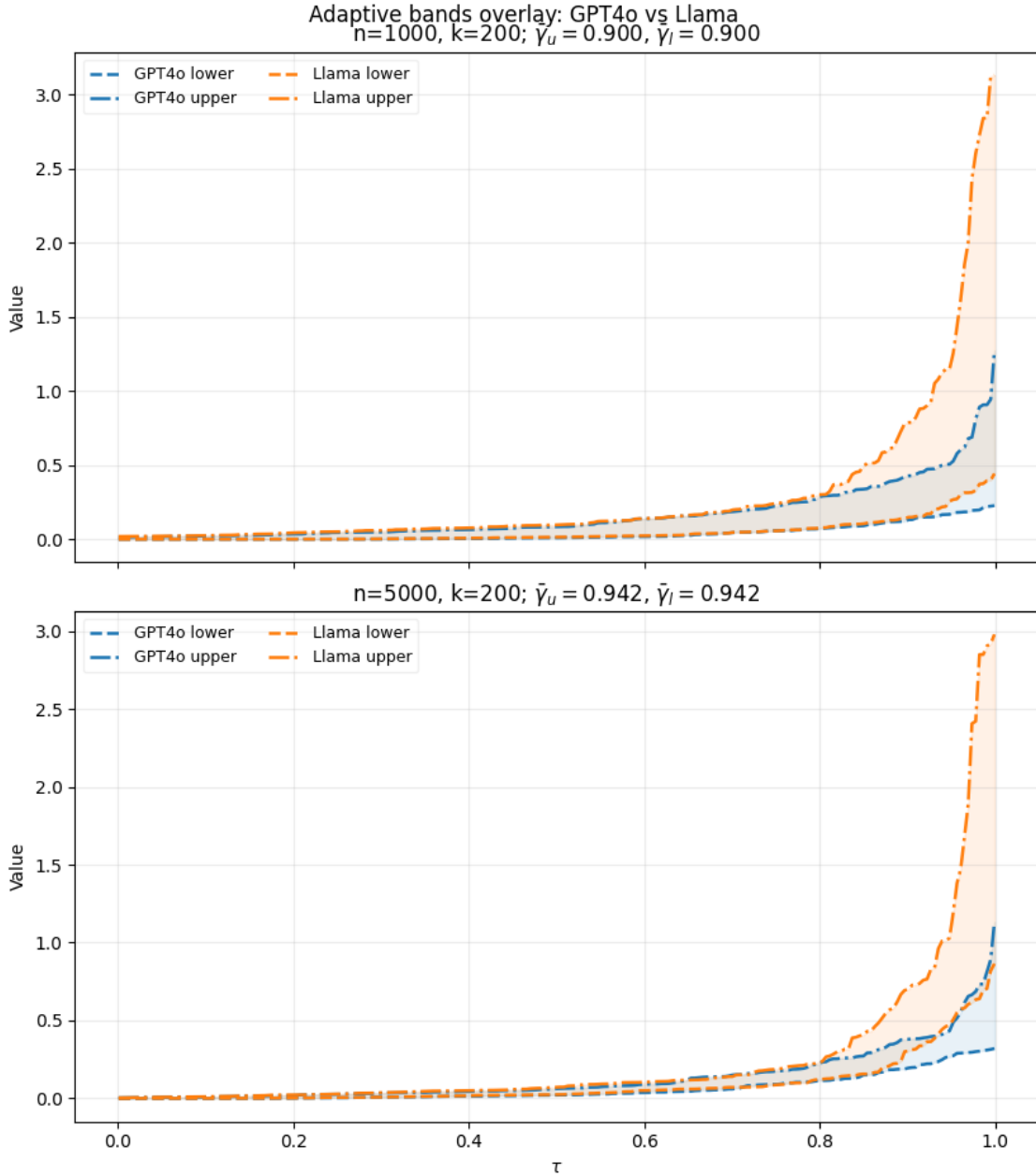


Figure 7: Confidence bands for GPT-4o and LLAMA 3.3. The top panel uses $n_j = 1000$, and $\bar{\gamma}_L = \bar{\gamma}_U = 0.900$; the bottom panel uses $n_j = 5000$, and $\bar{\gamma}_L = \bar{\gamma}_U = 0.942$, both with $k = 200$. In each panel, blue curves denote the lower and upper bands for GPT-4o, and orange curves for LLAMA 3.3 respectively.

The formal version of this result is presented in Theorem B.1 and its proof is deferred to Appendix B.4. The takeaway is that Theorems 3.1 and B.1 provide complementary tools for assessing simulator fidelity at the distributional level. Theorem 3.1 provides a one-sided, calibrated upper envelope for the population quantile curve, while Theorem B.1 augments this with a lower envelope, producing a confidence band that sandwiches the unknown quantile function $V(\tau)$. Figure 7 illustrates these bands for two subsample sizes $n_j \in \{1000, 5000\}$ and compares GPT-4O against LLAMA 3.3. Across both panels, the GPT-4O band lies systematically below the LLAMA 3.3 band over most quantile levels, with the separation becoming most pronounced in the upper tail. This pattern indicates that GPT-4O achieves systematically smaller calibrated discrepancy across scenarios and exhibits fewer extreme failures, and the conclusion is stable as n_j increases. Importantly, the comparison is fully data-driven: unlike oracle evaluations that rely on near-population human samples, the band construction does not require access to ground-truth discrepancies and can be carried out using only the observed heterogeneous batches.

6 Discussion

We develop a model-agnostic framework for profiling simulator fidelity through the quantile function of the sim-to-real discrepancy. Our approach makes no parametric assumptions about either the simulator or the real system, rigorously accounts for finite and heterogeneous sampling across scenarios, and yields calibrated, finite-sample guarantees at any target quantile level. The resulting fidelity profile supports a range of downstream summaries, from average performance to tail-risk measures that isolate rare but consequential failures. Finally, we demonstrate the practical value of the framework on real survey data, evaluating multiple LLM-based simulators and illustrating systematic, distribution-level differences in their alignment with human populations.

Despite its broad applicability, the method we introduce leaves several natural extensions. First, our framework targets *scenario-level population discrepancy*: for each scenario, the object of interest is a marginal population-level response distribution or derived parameter. As a result, the current formulation does not model respondent-level joint dependence across multiple questions. Second, our guarantees are developed for static per-scenario outputs under an i.i.d. scenario assumption, and do not yet cover fully dynamic simulators with temporal dependence, endogenous sampling, or distribution shift. Third, on the computational side, the main bottleneck is simulator-side generation: once real and simulated batches are available, our methodology computationally is lightweight, but expensive simulators may make sample generation itself the limiting factor. Finally, because the method relies on generic concentration inequalities and worst-case pseudo-discrepancies, the resulting envelope can be conservative when the number of scenarios m or the per-scenario sample sizes are small. In particular, our proof relies on DKW-type concentration—which can be loose for small m —together with a grid-uniform step that further weakens constants, so tightening these bounds is an immediate priority.

Acknowledgement

Kaizheng Wang’s research is supported by NSF grants DMS-2210907 and DMS-2515679 and a Data Science Institute seed grant SF-181 at Columbia University.

References

- AHER, G., ARRIAGA, R. I. and KALAI, A. T. (2023). Using large language models to simulate multiple humans and replicate human subject studies. In *Proceedings of the 40th International Conference on Machine Learning*. ICML'23, JMLR.org.
- ARGYLE, L. P., BUSBY, E. C., FULDA, N., GUBLER, J. R., RYTTING, C. and WINGATE, D. (2023). Out of one, many: Using language models to simulate human samples. *Political Analysis* **31** 337–351.
- BARDENET, R. and MAILLARD, O.-A. (2015). Concentration inequalities for sampling without replacement. *Bernoulli* **21** 1361 – 1385.
URL <https://doi.org/10.3150/14-BEJ605>
- BARTON, R. R., NELSON, B. L. and XIE, W. (2014). Quantifying input uncertainty via simulation confidence intervals. *INFORMS Journal on Computing* **26** 74–87.
- BATES, S., ANGELOPOULOS, A., LEI, L., MALIK, J. and JORDAN, M. (2021). Distribution-free, risk-controlling prediction sets. *Journal of the ACM (JACM)* **68** 1–34.
- BUDDE, C. E., HARTMANN, A., MEGGENDORFER, T., WEININGER, M. and WIENHÖFT, P. (2025). Statistical model checking beyond means: Quantiles, cvar, and the dkw inequality (extended version). *arXiv preprint arXiv:2509.11859* .
- CAO, Y., LIU, H., ARORA, A., AUGENSTEIN, I., RÖTTGER, P. and HERSHCOVICH, D. (2025). Specializing large language models to simulate survey response distributions for global populations. *arXiv preprint*.
URL <https://arxiv.org/abs/2502.07068>
- CHEN, M., LAM, H. and LIU, Z. (2024). Quantifying distributional input uncertainty via inflated kolmogorov-smirnov confidence band. *arXiv preprint arXiv:2403.09877* .
- CRANMER, K., BREHMER, J. and LOUPPE, G. (2020). The frontier of simulation-based inference. *Proceedings of the National Academy of Sciences* **117** 30055–30062.
- DURMUS, E., NGUYEN, K., LIAO, T. I., SCHIEFER, N., ASKELL, A., BAKHTIN, A., CHEN, C., HATFIELD-DODDS, Z., HERNANDEZ, D., JOSEPH, N. ET AL. (2023). Towards measuring the representation of subjective global opinions in language models. *arXiv preprint arXiv:2306.16388* .
- GAO, Y., LEE, D., BURTCHE, G. and FAZELPOUR, S. (2025). Take caution in using llms as human surrogates. *Proceedings of the National Academy of Sciences* **122** e2501660122.
URL <https://www.pnas.org/doi/abs/10.1073/pnas.2501660122>
- GRETTON, A., BORGWARDT, K. M., RASCH, M. J., SCHÖLKOPF, B. and SMOLA, A. (2012). A kernel two-sample test. *Journal of Machine Learning Research* **13** 723–773.
- HAERPFER, C., INGLEHART, R., MORENO, A., WELZEL, C., KIZILOVA, K., DIEZ-MEDRANO, J., LAGOS, M., NORRIS, P., PONARIN, E., PURANEN, B. ET AL. (2020). World values survey: Round seven – country-pooled datafile (2017–2020).
URL <https://doi.org/10.14281/18241.1>

- HE-YUEYA, J., MA, W. A., GANDHI, K., DOMINGUE, B. W., BRUNSKILL, E. and GOODMAN, N. D. (2024). Psychometric alignment: Capturing human knowledge distributions via language models. *arXiv preprint arXiv:2407.15645* .
- HEER, P., DERUNGS, C., HUBER, B., BÜNNING, F., FRICKER, R., STOLLER, S. and NIESEN, B. (2024). Comprehensive energy demand and usage data for building automation. *Scientific Data* **11** 469.
URL <https://doi.org/10.1038/s41597-024-03292-2>
- HOEFFDING, W. (1963). Probability inequalities for sums of bounded random variables. *Journal of the American Statistical Association* **58** 13–30.
URL <https://www.tandfonline.com/doi/abs/10.1080/01621459.1963.10500830>
- HUANG, C., WU, Y. and WANG, K. (2025). Uncertainty quantification for LLM-based survey simulations. In *Forty-second International Conference on Machine Learning*.
URL <https://openreview.net/forum?id=nY1Ge2wxtP>
- JEON, Y., CHU, Y., PASUPATHY, R. and SHASHAANI, S. (2024). Uncertainty quantification using simulation output: Batching as an inferential device.
URL <https://arxiv.org/abs/2311.04159>
- L.A., P. and BHAT, S. P. (2022). A wasserstein distance approach for concentration of empirical risk estimates. *Journal of Machine Learning Research* **23** 1–61.
URL <http://jmlr.org/papers/v23/20-965.html>
- LAM, H. (2022). Cheap bootstrap for input uncertainty quantification. In *Proceedings of the 2022 Winter Simulation Conference*. IEEE.
- LU, Y., HUANG, J., HAN, Y., YAO, B., BEI, S., GESI, J., XIE, Y., HE, Q., WANG, D. ET AL. (2025). Prompting is not all you need! evaluating llm agent simulation methodologies with real-world online customer behavior data. *arXiv preprint arXiv:2503.20749* .
- MACAL, C. (2016). Everything you need to know about agent-based modelling and simulation. *Journal of Simulation* **10** 144–156.
- MARDIA, J., JIAO, J., TÁNCZOS, E., NOWAK, R. D. and WEISSMAN, T. (2019). Concentration inequalities for the empirical distribution of discrete distributions: beyond the method of types. *Information and Inference: A Journal of the IMA* **9** 813–850.
URL <https://doi.org/10.1093/imaiai/iaz025>
- MASSART, P. (1990). The tight constant in the dvoretzky-kiefer-wolfowitz inequality. *The annals of Probability* 1269–1283.
- PAPAMAKARIOS, G., STERRATT, D. and MURRAY, I. (2019). Sequential neural likelihood: Fast likelihood-free inference with autoregressive flows. In *Proceedings of the Twenty-Second International Conference on Artificial Intelligence and Statistics* (K. Chaudhuri and M. Sugiyama, eds.), vol. 89 of *Proceedings of Machine Learning Research*. PMLR.
URL <https://proceedings.mlr.press/v89/papamakarios19a.html>
- PARK, J. S., O’BIEN, J., CAI, C. J., MORRIS, M. R., LIANG, P. and BERNSTEIN, M. S. (2023). Generative agents: Interactive simulacra of human behavior. In *Proceedings of the 36th annual acm symposium on user interface software and technology*.

- PENG, X. B., ANDRYCHOWICZ, M., ZAREMBA, W. and ABBEEL, P. (2018). Sim-to-real transfer of robotic control with dynamics randomization. In *2018 IEEE international conference on robotics and automation (ICRA)*. IEEE.
- RICHNER, P., HEER, P., LARGO, R., MARCHESI, E. and ZIMMERMANN, E. (2018). Nest – a platform for the acceleration of innovation in buildings. *Informes de la Construcción* **70** e255. Pp. 222.
- ROY, C. J. and OBERKAMPF, W. L. (2011). A comprehensive framework for verification, validation, and uncertainty quantification in scientific computing. *Computer Methods in Applied Mechanics and Engineering* **200** 2131–2144.
URL <https://www.sciencedirect.com/science/article/pii/S0045782511001290>
- SANTURKAR, S., DURMUS, E., LADHAK, F., LEE, C., LIANG, P. and HASHIMOTO, T. (2023a). Whose opinions do language models reflect? In *Proceedings of the 40th International Conference on Machine Learning*. ICML’23, JMLR.org.
- SANTURKAR, S., DURMUS, E., LADHAK, F., LEE, C., LIANG, P. and HASHIMOTO, T. (2023b). Whose opinions do language models reflect? In *Proceedings of the 40th International Conference on Machine Learning*. ICML’23, JMLR.org.
- SCHRAB, A., KIM, I., ALBERT, M., LAURENT, B., GUEDJ, B. and GRETTON, A. (2023). Mmd aggregated two-sample test. *Journal of Machine Learning Research* **24** 1–81.
URL <http://jmlr.org/papers/v24/21-1289.html>
- SNELL, J. C., ZOLLO, T. P., DENG, Z., PITASSI, T. and ZEMEL, R. (2022). Quantile risk control: A flexible framework for bounding the probability of high-loss predictions. *arXiv preprint arXiv:2212.13629* .
- TOBIN, J., FONG, R., RAY, A., SCHNEIDER, J., ZAREMBA, W. and ABBEEL, P. (2017). Domain randomization for transferring deep neural networks from simulation to the real world. In *2017 IEEE/RSJ international conference on intelligent robots and systems (IROS)*. IEEE.
- VOVK, V., GAMMERMAN, A. and SHAFER, G. (2005). *Algorithmic Learning in a Random World*. Springer-Verlag, Berlin, Heidelberg.
- WANG, Z., LAMB, A., SAVELIEV, E., CAMERON, P., ZAYKOV, J., HERNANDEZ-LOBATO, J. M., TURNER, R. E., BARANIUK, R. G., CRAIG BARTON, E., PEYTON JONES, S., WOODHEAD, S. and ZHANG, C. (2021). Results and insights from diagnostic questions: The neurips 2020 education challenge. In *Proceedings of the NeurIPS 2020 Competition and Demonstration Track* (H. J. Escalante and K. Hofmann, eds.), vol. 133 of *Proceedings of Machine Learning Research*. PMLR.
URL <https://proceedings.mlr.press/v133/wang21a.html>
- WESTWOOD, S. J. (2025). The potential existential threat of large language models to online survey research. *Proceedings of the National Academy of Sciences* **122** e2518075122. Epub 2025-11-20.
- ZHANG, L., ZHOU, L., REN, L. and LAILI, Y. (2019). Modeling and simulation in intelligent manufacturing. *Computers in Industry* **112** 103123.
URL <https://www.sciencedirect.com/science/article/pii/S0166361519303239>

ZHAO, W., MONDAL, D., TANDON, N., DILLION, D., GRAY, K. and GU, Y. (2024). Worldvalues-bench: A large-scale benchmark dataset for multi-cultural value awareness of language models. URL <https://arxiv.org/abs/2404.16308>

A Technical Lemmas

Lemma A.1. (*Dvoretzky-Kiefer-Wolfowitz (DKW) Inequality via [Massart \(1990\)](#)*)

Let X_1, X_2, \dots, X_n be i.i.d. real-valued random variables with cumulative distribution function (CDF) F^* , and let \hat{F}_n be the empirical distribution function defined by

$$\hat{F}_n(x) := \frac{1}{n} \sum_{i=1}^n \mathbf{1}\{X_i \leq x\}.$$

Then, for any $\varepsilon > 0$,

$$\mathbb{P} \left(\sup_{x \in \mathbb{R}} |\hat{F}_n(x) - F^*(x)| > \varepsilon \right) \leq 2e^{-2n\varepsilon^2}.$$

Equivalently, for any confidence level $\delta \in (0, 1)$, with probability at least $1 - \delta$,

$$\sup_{x \in \mathbb{R}} |\hat{F}_n(x) - F^*(x)| \leq \sqrt{\frac{1}{2n} \log \left(\frac{2}{\delta} \right)}.$$

Lemma A.2. [*Hoeffding (additive) via [Hoeffding \(1963\)](#)*]

Let $Z_1, \dots, Z_n \in [0, 1]$ be independent, $T = \sum_{i=1}^n Z_i$, and $\mu = \mathbb{E}[T]$. For any $t \in [0, \mu]$,

$$\mathbb{P}(T \leq \mu - t) \leq \exp \left(-\frac{2t^2}{\sum_{i=1}^n (1 - 0)^2} \right) = \exp \left(-\frac{2t^2}{n} \right).$$

Lemma A.3. [*Chernoff–Hoeffding for one-parameter exponential family*]

Let X_1, \dots, X_n be i.i.d. with density (or mass) in the one-parameter canonical exponential family

$$p_\theta(x) = \exp\{\theta T(x) - A(\theta)\} h(x), \quad \theta \in \Theta,$$

where $T(x)$ is the sufficient statistic, $A(\theta)$ is the log-partition function (convex, differentiable on Θ), and the mean map is $\mu(\theta) := \mathbb{E}_\theta[T(X)] = A'(\theta)$. Assume Θ is an open interval and all quantities below are finite.

Define the empirical mean of the sufficient statistic

$$\bar{T}_n = \frac{1}{n} \sum_{i=1}^n T(X_i).$$

For each t in the range of \bar{T}_n let θ_t be the (unique) canonical parameter satisfying $\mu(\theta_t) = t$. Then for any $\varepsilon > 0$,

$$\mathbb{P}(D(p_{\theta_{\bar{T}_n}} \| p_\theta) > \varepsilon) \leq 2e^{-n\varepsilon}$$

Proof:

Define the shifted log-MGF under p_θ ,

$$\psi_\theta(\lambda) := \log \mathbb{E}_\theta [e^{\lambda T(X)}] = A(\theta + \lambda) - A(\theta),$$

where the displayed equality follows from the exponential-family form (for λ in the domain where the expectation is finite). For an attainable mean m denote θ_m as the unique solution of $\mu(\theta_m) = m$.

By adopting the one-sided Chernoff bound, for any real λ such that expectations exist and any $m \in \mathbb{R}$,

$$\begin{aligned}\mathbb{P}_\theta(\bar{T}_n \geq m) &= \mathbb{P}(e^{\lambda n \bar{T}_n} \geq e^{\lambda n m}) \\ &\leq e^{-\lambda n m} \mathbb{E}_\theta[e^{\lambda n \bar{T}_n}] \\ &= \exp(-n(\lambda m - \psi_\theta(\lambda))).\end{aligned}$$

Optimizing over λ gives the Chernoff bound

$$\mathbb{P}_\theta(\bar{T}_n \geq m) \leq \exp(-n\psi_\theta^*(m)), \implies \psi_\theta^*(m) := \sup_{\lambda \in \mathbb{R}} \{\lambda m - \psi_\theta(\lambda)\},$$

where $\psi_\theta^*(m)$ is the Fenchel-Legendre transform of log-MGF. A symmetric argument with $\lambda < 0$ yields the lower-tail bound

$$\mathbb{P}_\theta(\bar{T}_n \leq m) \leq \exp(-n\psi_\theta^*(m)).$$

We next link the Fenchel-Legendre transform to KL-Divergence using exponential tilting. First, adopting change of variables $\eta = \theta + \lambda$. Then

$$\begin{aligned}\psi_\theta^*(m) &= \sup_{\eta} \{\langle \eta - \theta, m \rangle - (A(\eta) - A(\theta))\} \\ &= A(\theta) + A^*(m) - \langle \theta, m \rangle,\end{aligned}$$

where $A^*(m) = \sup_{\eta} \{\langle \eta, m \rangle - A(\eta)\}$ is the convex conjugate of A . When m is attainable, the supremum is achieved at $\eta = \theta_m$, and therefore

$$\psi_\theta^*(m) = \langle \theta_m - \theta, m \rangle - (A(\theta_m) - A(\theta)).$$

But for exponential-family densities one has the following direct algebraic identity for the KL:

$$\begin{aligned}D(p_{\theta_1} \| p_{\theta_2}) &= \mathbb{E}_{\theta_1} \left[\log \frac{p_{\theta_1}(X)}{p_{\theta_2}(X)} \right] \\ &= \mathbb{E}_{\theta_1} [(\theta_1 - \theta_2)T(X) - (A(\theta_1) - A(\theta_2))] \\ &= (\theta_1 - \theta_2) \mathbb{E}_{\theta_1}[T(X)] - (A(\theta_1) - A(\theta_2)).\end{aligned}$$

Taking $\theta_1 = \theta_m$ and $\theta_2 = \theta$ (so $\mathbb{E}_{\theta_1}[T] = m$) yields

$$\psi_\theta^*(m) = D(p_{\theta_m} \| p_\theta).$$

Combining this with the one-sided Chernoff-bound above yields the one-sided KL-form Chernoff bounds

$$\begin{aligned}\mathbb{P}_\theta(\bar{T}_n \geq m) &\leq e^{-nD(p_{\theta_m} \| p_\theta)}, \\ \mathbb{P}_\theta(\bar{T}_n \leq m) &\leq e^{-nD(p_{\theta_m} \| p_\theta)}.\end{aligned}$$

Fix $\varepsilon > 0$. Because $A'' > 0$ the function $m \mapsto D(p_{\theta_m} \| p_\theta)$ is continuous, strictly convex and has a unique minimum 0 at $m = A'(\theta)$. Thus the sublevel set $\{m : D(p_{\theta_m} \| p_\theta) < \varepsilon\}$ is an open interval (m_-, m_+) ; equivalently

$$\{m : D(p_{\theta_m} \| p_\theta) \geq \varepsilon\} = (-\infty, m_-] \cup [m_+, \infty).$$

Hence

$$\{D(p_{\theta_{\bar{T}_n}} \| p_\theta) \geq \varepsilon\} \subseteq \{\bar{T}_n \leq m_-\} \cup \{\bar{T}_n \geq m_+\}.$$

Applying the one-sided KL bounds at m_\pm (each equals ε) and using the union bound gives

$$\mathbb{P}(D(p_{\theta_{\bar{T}_n}} \| p_\theta) \geq \varepsilon) \leq e^{-n\varepsilon} + e^{-n\varepsilon} = 2e^{-n\varepsilon},$$

which proves the lemma.

Lemma A.4. (*Chernoff-Hoeffding Inequality*)

Let $X_1, \dots, X_n \sim \text{Ber}(\tilde{p})$ be i.i.d. Bernoulli random variables with unknown mean \tilde{p} , and define the empirical mean as

$$\bar{X}_n = \frac{1}{n} \sum_{i=1}^n X_i.$$

Then for any $\varepsilon > 0$,

$$\mathbb{P}(D(\bar{X}_n \| \tilde{p}) > \varepsilon) \leq 2e^{-n\varepsilon},$$

where $D(p \| q)$ is the Kullback-Leibler divergence between Bernoulli distributions with parameters p and q .

Proof: Via Lemma A.3.

Lemma A.5 (Multinomial Chernoff-Hoeffding Bound via [Mardia et al. \(2019\)](#)). For all $d \leq (\frac{nC_0}{4})^{\frac{1}{3}}$ and $P \in \mathcal{M}_k$, the following holds with the universal constants $C_0 = \frac{e^3}{2\pi} \approx 3.1967$, for any $\epsilon > 0$,

$$\Pr(D(\hat{P}_{n,d} \| P) \geq \epsilon) \leq 2(d-1)e^{-\frac{n\epsilon}{d-1}}.$$

Lemma A.6 (Wasserstein distance bound via [L.A. and Bhat \(2022\)](#)). Let X be a sub-Gaussian r.v. with parameter σ . Let F denote the CDF of X . Then, for every $n \geq 1$ and ε such that $\frac{512\sigma}{\sqrt{n}} < \varepsilon < \frac{512\sigma}{\sqrt{n}} + 16\sigma\sqrt{e}$, we have

$$\mathbb{P}(W_1(F_n, F) > \varepsilon) \leq \exp\left(-\frac{n}{256\sigma^2 e} \left(\varepsilon - \frac{512\sigma}{\sqrt{n}}\right)^2\right),$$

where e is Euler's number.

Lemma A.7 (Order-statistic thresholding). Let $x_1, \dots, x_m \in \mathbb{R}$ and let $x_{(1)} \leq \dots \leq x_{(m)}$ be their order statistics. Fix a threshold $\tau \in \mathbb{R}$ and an integer $N \in \{1, \dots, m\}$. If at least N of the sample values are at least τ , i.e. $|\{j : x_j \geq \tau\}| \geq N$, then

$$x_{(m-N+1)} \geq \tau.$$

(Equivalently, if at least N of the x_j are strictly larger than τ , the same conclusion holds.)

Proof:

Suppose, for contradiction, that $x_{(m-N+1)} < \tau$. Then all of the first $m - N + 1$ order statistics are strictly less than τ , so there are at most $m - (m - N + 1) = N - 1$ indices j with $x_j \geq \tau$, contradicting $|\{j : x_j \geq \tau\}| \geq N$. Hence $x_{(m-N+1)} \geq \tau$.

B Proof to Theorem 3.1 and 5.1

B.1 Proof for Theorem 3.1

We condition on $\mathcal{G}_j := \sigma(\psi_j, \hat{q}_j, n_j)$ and $\mathcal{G} := \sigma(\{\mathcal{G}_j\}_{j=1}^m)$. By Assumption 3.1, conditional on \mathcal{G} the additional randomness used to construct \hat{p}_j (hence $\hat{\Delta}_j$ and the indicators below) is independent across j . For brevity, we abuse notation and write $p(\psi_j), q(\psi_j)$ as p_j, q_j , and similarly \hat{p}, \hat{q} . We also ignore the superscript k to simplify the proof, and discussions on the dependence on k can be found in Section 3. Split $\delta = \delta_{\text{DKW}} + \delta_{\text{al}} + \delta_{\text{cnt}}$ with $\delta_{\text{DKW}} = \delta_{\text{al}} = \delta_{\text{cnt}} = \delta/3$, and union bound the three events defined below.

We first show an idealized case where we have access to the oracle p_j , and hence can obtain the actual sim-to-real discrepancy Δ_j . Under this setting, we can directly define $F(t) := \mathbb{P}_{\psi \sim \Psi}(\Delta(\psi) \leq t)$ and

$$\bar{F}_m(t) := \frac{1}{m} \sum_{j=1}^m \mathbf{1}\{\Delta_j \leq t\}, \quad \bar{V}_m(u) := \inf\{t : \bar{F}_m(t) \geq u\}.$$

By the DKW inequality (Lemma A.1), the following event

$$\mathcal{E}_{\text{DKW}} := \left\{ \sup_t |\bar{F}_m(t) - F(t)| \leq \varepsilon_m(\delta) \right\},$$

occur with probability at least $1 - \delta_{\text{DKW}}$, where $\varepsilon_m(\delta) = \sqrt{\frac{\log(6/\delta)}{2m}}$. On \mathcal{E}_{DKW} , for every $u \in (0, 1)$,

$$\mathbb{P}_{\psi \sim \Psi}(\Delta(\psi) \leq \bar{V}_m(u) \mid \mathcal{D}) \geq u - \varepsilon_m(\delta). \quad (\text{B.1})$$

Now in our dataset, we do not have access to the above oracle Δ_j . Therefore, we control for Δ_j using the pseudo-discrepancy $\hat{\Delta}_j$. Define $Y_j := \mathbf{1}\{\hat{\Delta}_j \geq \Delta_j\}$. By the coverage of $\mathcal{C}_j(\hat{p}_j, \gamma_j)$ and the definition of $\hat{\Delta}_j$,

$$\mathbb{P}(Y_j = 1 \mid \mathcal{G}_j) \geq \gamma_j.$$

For $r = 1, \dots, m$, let $\alpha_r := r/m$ and define the oracle right-tail set

$$S_r := \{j \in [m] : \Delta_j \geq \bar{V}_m(1 - \alpha_r)\}, \quad s_r := |S_r|.$$

By definition of empirical quantiles, $s_r \geq r$. We then introduce link from the oracle set to the pseudo-discrepancies by defining counts

$$T_r := \sum_{j \in S_r} Y_j, \quad U_r := |\{j : \hat{\Delta}_j \geq \bar{V}_m(1 - \alpha_r)\}|.$$

By construction, $U_r \geq T_r$. Notice that U_r will give us the amount of $\hat{\Delta}$ required to achieve the tail count of the empirical oracle quantile function, hence we will try to create a lower bound for U_r via T_r .

Under Assumption 3.1, $\{n_j\}$ are deterministic, and hence independent of $\{\psi_j\}$ and therefore independent of $\{\Delta_j\}$; consequently, the random index set S_r (which is measurable w.r.t. $\{\Delta_j\}_{j=1}^m$) is independent of the vector $(\gamma_1, \dots, \gamma_m)$. Conditional on the realized multiset $\{\gamma_j\}_{j=1}^m$, the subcollection $\{\gamma_j : j \in S_r\}$ is thus a simple random sample without replacement from $\{\gamma_j\}_{j=1}^m$. By Hoeffding–Serfling [Bardenet and Maillard \(2015\)](#), for each r and each $\tau > 0$,

$$\mathbb{P}\left(\frac{1}{s_r} \sum_{j \in S_r} \gamma_j \leq \bar{\gamma}_m - \tau\right) \leq \exp(-2s_r\tau^2).$$

Set

$$\tau_r := \sqrt{\frac{\log(m/\delta_{\text{al}})}{2s_r}} \leq \sqrt{\frac{\log(3m/\delta)}{2r}} =: \varepsilon_{\text{al}}(\alpha_r, \delta),$$

and union bound over $r = 1, \dots, m$ to obtain an event \mathcal{E}_{al} with $\mathbb{P}(\mathcal{E}_{\text{al}}) \geq 1 - \delta_{\text{al}}$ on which, for all r ,

$$\sum_{j \in S_r} \gamma_j \geq s_r(\bar{\gamma}_m - \varepsilon_{\text{al}}(\alpha_r, \delta)). \quad (\text{B.2})$$

Conditional on \mathcal{G} , the indicators $\{Y_j\}_{j=1}^m$ are independent and bounded in $[0, 1]$, so Lemma A.2 implies that for any $t > 0$,

$$\mathbb{P}\left(T_r \leq \mathbb{E}[T_r \mid \mathcal{G}] - t \mid \mathcal{G}\right) \leq \exp\left(-\frac{2t^2}{s_r}\right).$$

Since $\mathbb{E}[T_r \mid \mathcal{G}] = \sum_{j \in S_r} \mathbb{E}[Y_j \mid \mathcal{G}] \geq \sum_{j \in S_r} \gamma_j$, choose

$$c_m := \sqrt{\frac{1}{2} \log \frac{m}{\delta_{\text{cnt}}}} \leq \sqrt{\frac{1}{2} \log \frac{3m}{\delta}}, \quad t_r := c_m \sqrt{s_r}.$$

Then $\mathbb{P}(T_r \geq \sum_{j \in S_r} \gamma_j - c_m \sqrt{s_r} \mid \mathcal{G}) \geq 1 - \delta_{\text{cnt}}/m$. A union bound over $r = 1, \dots, m$ yields an event \mathcal{E}_{cnt} with $\mathbb{P}(\mathcal{E}_{\text{cnt}}) \geq 1 - \delta_{\text{cnt}}$ on which, for all r ,

$$T_r \geq \sum_{j \in S_r} \gamma_j - c_m \sqrt{s_r}. \quad (\text{B.3})$$

Combining (B.2) and (B.3) gives, for all r ,

$$T_r \geq s_r(\bar{\gamma}_m - \varepsilon_{\text{al}}(\alpha_r, \delta)) - c_m \sqrt{s_r}$$

on the event $\mathcal{E}_{\text{al}} \cap \mathcal{E}_{\text{cnt}}$. Using $s_r \geq r = m\alpha_r$ and $c_m/\sqrt{m} = b_m(\delta)$ yields

$$U_r \geq T_r \geq m\left((\bar{\gamma}_m - \varepsilon_{\text{al}}(\alpha_r, \delta))\alpha_r - b_m(\delta)\sqrt{\alpha_r}\right).$$

Equivalently, at least $m\alpha_{\text{eff}}(\alpha_r)$ of the $\hat{\Delta}_j$'s exceed $\bar{V}_m(1 - \alpha_r)$, hence

$$\hat{V}_m(1 - \alpha_{\text{eff}}(\alpha_r)) \geq \bar{V}_m(1 - \alpha_r), \quad r = 1, \dots, m. \quad (\text{B.4})$$

Finally, we work on $\mathcal{E}_{\text{DKW}} \cap \mathcal{E}_{\text{al}} \cap \mathcal{E}_{\text{cnt}}$, which has probability at least $1 - \delta$ by the union bound. Fix any $\alpha \in (0, 1)$ and let $\alpha_+ := \lceil m\alpha \rceil / m$. By discretization, $\alpha_{\text{eff}}(\alpha) = \alpha_{\text{eff}}(\alpha_+)$. Applying (B.4) at $r = \lceil m\alpha \rceil$ yields

$$\hat{V}_m(1 - \alpha_{\text{eff}}(\alpha)) = \hat{V}_m(1 - \alpha_{\text{eff}}(\alpha_+)) \geq \bar{V}_m(1 - \alpha_+).$$

Applying (B.1) with $u = 1 - \alpha_+$ gives

$$\begin{aligned} \mathbb{P}_{\psi \sim \Psi}(\Delta(\psi) \leq \bar{V}_m(1 - \alpha_+) \mid \mathcal{D}) &\geq 1 - \alpha_+ - \varepsilon_m(\delta) \\ &\geq 1 - \alpha - \varepsilon_m(\delta) - \frac{1}{m}. \end{aligned}$$

Monotonicity in the threshold implies (3.6), hence shown. \square

Corollary B.1. *Adopt the setting of Theorem (3.1) and set $\gamma_j = \gamma$ for all $j \in [m]$. Then, for any $\alpha \in (0, 1)$, with probability at least $1 - \eta$ over \mathcal{D} , we have*

$$\mathbb{P}_{\psi \sim \Psi}\left(\Delta_{\psi}^{(k)} \leq \hat{V}_m(1 - \gamma\alpha) \mid \mathcal{D}\right) \geq 1 - \alpha - \frac{\varepsilon_{\gamma}(\alpha, m, \eta)}{\sqrt{m}}, \quad (\text{B.5})$$

where the remainder ε_{γ} is $O(\sqrt{(\log m)/m})$ as $m \rightarrow \infty$.

B.2 Proof for Corollary B.1:

One method is to directly adopt Theorem 3.1's proof and readjust the remainder term. Here we adopt a slightly alternative method. We first consider a fixed level of confidence $\bar{\alpha}$, then extend to $\bar{\alpha}$ holding uniformly across $(0, 1)$. Throughout the proof, $\alpha \in (0, 1)$ denotes a generic quantile index (a function argument) and is distinct from the target coverage level $\bar{\alpha}$.

As a setup, we work conditionally on $\mathcal{G}_j := \sigma(\psi_j, \hat{q}_j, n_j)$, $\mathcal{G} := \sigma(\{\mathcal{G}_j\}_{j=1}^m)$. Here \mathcal{G}_j is the σ -field collecting all "human-side" information for scenario j . Thus $\mathcal{G} := \sigma(\{\mathcal{G}_j\}_{j=1}^m)$ represents the joint information from all scenarios that we treat as fixed when analyzing the remaining randomness coming from the estimation noise in \hat{p}_j . For brevity, we abuse notation and write $p(\psi_j), q(\psi_j)$ as p_j, q_j , and similarly \hat{p}, \hat{q} . We also ignore the superscript k to simplify the proof, and discussions on the dependence on k can be found in Section 3. In addition, for any quantities $\{\Delta_j\}_{j=1}^m$, we denote the sorted version as $\{\Delta_{(i)}\}_{i=1}^m$, ie. $\Delta_{(1)} \leq \dots \leq \Delta_{(m)}$. For any sequence $\{\Delta_j\}_{j=1}^m$, let $\Delta_{(1)} \leq \dots \leq \Delta_{(m)}$ denote its order statistics.

We seek the quantile function of $\Delta_j = L(p_j, \hat{q}_j)$, but only observe the estimators (\hat{p}_j, \hat{q}_j) . Note that the sequence $\{\Delta_j\}_{j=1}^m$ is i.i.d., since the simulator budget k is fixed and each scenarios $\{\psi_j\}$ are i.i.d. as assumed in Section 2.

Let $\bar{V}_m(\alpha) = \inf\{t : \bar{F}_m(t) \geq \alpha\} = \Delta_{(\lceil m\alpha \rceil)}$ be the empirical α quantile of $\{\Delta_j\}_{j=1}^m$, where $\bar{F}_m(x) = \frac{1}{m} \sum_{j=1}^m \mathbb{I}(\Delta_j \leq x)$. By Lemma A.1, with probability $1 - \delta$:

$$\mathbb{P}_{\psi \sim \Psi}(L(p(\psi), \hat{q}(\psi)) \leq \bar{V}_m(1 - \frac{\bar{\alpha}}{2}) | \mathcal{D}) \geq 1 - \frac{\bar{\alpha}}{2} - \sqrt{\frac{\log(2/\delta)}{2m}} \quad (\text{B.6})$$

and we would have our desired bound.

However, for the above argument to hold, we would need to know p_j , instead we only have the estimated \hat{p}_j . Therefore, we instead construct a pseudo-gaps using confidence sets with coverage level γ , and define the two gap terms as

$$\begin{cases} \Delta_j = L(p_j, \hat{q}_j) & , \text{ i.i.d., yet unobservable} \\ \hat{\Delta}_j := \sup_{u \in \mathcal{C}_j(\hat{p}_j, \gamma)} L(u, \hat{q}_j) & , \text{ Not i.i.d., yet observable,} \end{cases}$$

where $\mathcal{C}_j(\hat{p}_j, \gamma) \subset \Theta$ are data-driven confidence sets satisfying $\mathbb{P}(p_j \in \mathcal{C}_j(\hat{p}_j, \gamma) | \psi_j, n_j) \geq \gamma$.

By Assumption 3.2 and the compactness of the confidence set $\mathcal{C}_j(\hat{p}_j, \gamma) \subset \Theta$, Berge's maximum theorem guarantees that the supremum in the definition of $\hat{\Delta}_j$ is attained, hence $\hat{\Delta}_j$ is well defined. Therefore, by the coverage property of \mathcal{C}_j , we have $\mathbb{P}(\hat{\Delta}_j \geq \Delta_j | \mathcal{G}_j \cup \sigma(\gamma)) \geq \gamma$, and we get $\forall j$

$$\mathbb{P}(\hat{\Delta}_j \geq \Delta_j | \mathcal{G}_j) \geq \gamma. \quad (\text{B.7})$$

Furthermore, by the tower property and $\gamma \perp\!\!\!\perp \mathcal{G}_j$,

$$\mathbb{P}(\hat{\Delta}_j \geq \Delta_j) = \mathbb{E}[\mathbb{P}(\hat{\Delta}_j \geq \Delta_j | \mathcal{G}_j)] \geq \gamma.$$

Moreover, by the above discussion, conditional on \mathcal{G} , the indicators $Y_j = \mathbf{1}\{\hat{\Delta}_j \geq \Delta_j\}$ are independent across j . We will use $\{\hat{\Delta}_j\}_{j=1}^m$ to create an upper bound of $\bar{V}_m(1 - \alpha)$, which along side (B.6) will give us our desired envelope. Intuitively, we want to find a larger quantile of $\hat{\Delta}_j$ and with (B.7), we can claim an upper bound of $\bar{V}_m(1 - \alpha)$ with high probability.

First, define $S_\alpha := \{j \in [m] : \Delta_j \geq \bar{V}_m(1 - \alpha)\}$ and $s := |S_\alpha|$. By definition of the empirical $(1 - \alpha)$ -quantile $\bar{V}_m(1 - \alpha)$, at most a fraction $(1 - \alpha)$ of the sample can lie strictly below it. More precisely,

$$|\{j \in [m] : \Delta_j < \bar{V}_m(1 - \alpha)\}| \leq \lfloor m(1 - \alpha) \rfloor.$$

Therefore the number of indices with $\Delta_j \geq \bar{V}_m(1 - \alpha)$ is at least

$$s \geq m - \lfloor m(1 - \alpha) \rfloor = \lceil m\alpha \rceil \geq \lfloor m\alpha \rfloor.$$

We next define $Y_j = \mathbb{I}(\hat{\Delta}_j \geq \Delta_j)$. By (B.7): $\mathbb{P}(Y_j = 1 | \mathcal{G}) \geq \gamma$. Next, define $T_\alpha = \{j \in S_\alpha : \hat{\Delta}_j \geq \Delta_j\} = \{j \in S_\alpha : Y_j = 1\} = \{j : \hat{\Delta}_j \geq \Delta_j \geq \bar{V}_m(1 - \alpha)\}$. First, we calculate $\mathbb{E}[T_\alpha]$:

$$\mathbb{E}[T_\alpha | \mathcal{G}] = \mathbb{E}\left[\sum_{j \in S_\alpha} Y_j | \mathcal{G}\right] = \sum_{j \in S_\alpha} \mathbb{P}(Y_j | \mathcal{G}) \geq \gamma s.$$

Lemma A.2 implies that for any $\delta \in [0, \gamma s]$, we have:

$$\mathbb{P}\left(|T_\alpha| \leq \gamma s - t | \mathcal{G}\right) \leq \mathbb{P}\left(|T_\alpha| \leq \mathbb{E}[T_\alpha] - t | \mathcal{G}\right) \leq \exp\left(-\frac{2t^2}{s}\right),$$

where we applied $\mathbb{E}[T_\alpha | \mathcal{G}] \geq \gamma s$ in the first inequality. By setting $t = c\sqrt{s}$:

$$\mathbb{P}\left(|T_\alpha| \leq \gamma s - t | \mathcal{G}\right) \leq \exp(-2c^2) \tag{B.8}$$

With this bound, we can link the actual set of indices we have interest, ie. $U_\alpha = \{j : \hat{\Delta}_j \geq \bar{V}_m(1 - \alpha)\}$ to T_α . By construction, $T_\alpha \subseteq U_\alpha$, hence by (B.8), with probability greater than $1 - \exp(-2c^2)$:

$$|U_\alpha| \geq |T_\alpha| \geq \gamma s - c\sqrt{s},$$

which implies at least $\gamma s - c\sqrt{s}$ of the $\hat{\Delta}_j$'s are larger than $\bar{V}_m(1 - \alpha)$ with high probability.

We now analyze what coverage guarantee can we get for the inner probability via order statistics for any α . Set $N := \lfloor \gamma s - c\sqrt{s} \rfloor$ and define $\hat{V}_m(\alpha) := \inf\{t : \hat{F}_m(t) \geq \alpha\} = \Delta_{(\lceil m\alpha \rceil)}$, where $\hat{F}(x) = \frac{1}{m} \sum_{j=1}^m \mathbb{I}(\hat{\Delta}_j \leq x)$. If at least N sample values exceed $\bar{V}_m(1 - \alpha)$, then by order-statistics calculus (Lemma A.7)

$$\hat{V}_m(1 - \alpha) = \hat{\Delta}_{(m - \lfloor m\alpha \rfloor)} \geq \bar{V}_m(1 - \alpha_{\text{eff}}),$$

whenever α_{eff} is chosen so that $N \geq \lfloor m\alpha \rfloor + 1$ holds when $s \geq \lfloor m\alpha_{\text{eff}} \rfloor + 1$.

A sufficient condition for the above to satisfy is

$$\gamma m \alpha_{\text{eff}} - c\sqrt{m\alpha_{\text{eff}}} - 1 \geq m\alpha.$$

Define $\alpha_{\text{eff}}(\alpha, c, m) := \inf\{x \in (0, 1) : \gamma x - c\sqrt{\frac{x}{m}} - \frac{1}{m} \geq \alpha\}$. Writing $y = \sqrt{x}$, this is equivalent to $\gamma y^2 - \frac{c}{\sqrt{m}}y - \left(\frac{1}{m} + \alpha\right) \geq 0$, so the minimal admissible y is

$$y^* = \frac{c/\sqrt{m} + \sqrt{c^2/m + 4\gamma\alpha + 4\gamma/m}}{2\gamma}, \quad \alpha_{\text{eff}}(\alpha, c, m) = (y^*)^2.$$

Thus, we define

$$\mathcal{E}_\alpha := \left\{ \hat{V}_m(1 - \alpha) \geq \bar{V}_m(1 - \alpha_{\text{eff}}(\alpha, c, m)) \right\}, \tag{B.9}$$

then $\mathbb{P}(\mathcal{E}_\alpha) \geq 1 - e^{-2c^2}$.

Next, we apply (B.6) at level $1 - \alpha_{\text{eff}}(\bar{\alpha}, c, m)$:

$$\mathbb{P}_{\psi \sim \Psi}\left(\Delta_\psi \leq \bar{V}_m(1 - \alpha_{\text{eff}}) \mid \mathcal{D}\right) \geq 1 - \alpha_{\text{eff}}(\bar{\alpha}, c, m) - \varepsilon_m(\delta).$$

On $\mathcal{E}_{\bar{\alpha}}$ in (B.9), $\bar{V}_m(1 - \alpha_{\text{eff}}) \leq \hat{V}_m(1 - \bar{\alpha})$. Hence,

$$\mathbb{P}_{\psi \sim \Psi}(\Delta_\psi \leq \hat{V}_m(1 - \bar{\alpha}) | \mathcal{D}) \geq 1 - \alpha_{\text{eff}}(\bar{\alpha}, c, m) - \varepsilon_m(\delta), \quad (\text{B.10})$$

with outer probability at least $1 - \delta - e^{-2c^2}$.

The exact algebraic form is

$$\begin{aligned} \alpha_{\text{eff}}(\bar{\alpha}, c, m) &= \frac{\left(\frac{c}{\sqrt{m}} + \sqrt{\frac{c^2}{m} + 4\gamma\bar{\alpha} + \frac{4\gamma}{m}}\right)^2}{4\gamma^2} \\ &= \frac{\bar{\alpha}}{\gamma} + \frac{c}{\gamma\sqrt{m}} \sqrt{4\gamma\bar{\alpha} + \frac{c^2+4\gamma}{m}} + \frac{c^2}{2\gamma^2 m} + \frac{1}{\gamma m}. \end{aligned}$$

Therefore, as $m \rightarrow \infty$, $\alpha_{\text{eff}}(\alpha, c, m) = \frac{\alpha}{\gamma} + c\sqrt{4\alpha/\gamma m} + O(m^{-1})$.

We have shown that for any target level α and choice of $c > 0$, the preceding argument yields a high-probability concentration bound based on $\{\hat{\Delta}_j\}_{j=1}^m$. We now extend the guarantee to hold *uniformly* over all α . Fix $c > 0$ and $\delta \in (0, 1)$. For the grid $\alpha_r := r/m$ ($r = 1, \dots, m$), let

$$\begin{aligned} \mathcal{E}_{\text{DKW}} &:= \left\{ \sup_x |\hat{F}_m(x) - F^*(x)| \leq \varepsilon_m(\delta) \right\} \\ \mathcal{E}_r &:= \left\{ (\text{B.10}) \text{ holds with } \alpha = \alpha_r \right\}. \end{aligned}$$

By DKW, $\mathbb{P}(\mathcal{E}_{\text{DKW}}) \geq 1 - \delta$, and by the fixed-level argument, $\mathbb{P}(\mathcal{E}_r) \geq 1 - e^{-2c^2}$ for each r . Hence, by a union bound,

$$\mathbb{P}\left(\mathcal{E}_{\text{DKW}} \cap \bigcap_{r=1}^m \mathcal{E}_r\right) \geq 1 - \delta - me^{-2c^2}.$$

For any $\alpha \in (0, 1)$ let $r = \lceil m\alpha \rceil$ and denote $\alpha_+ := \alpha_r = r/m \in [\alpha, \alpha + 1/m]$. Since the empirical quantile is piecewise constant on the m -grid,

$$\hat{V}_m(1 - \alpha) = \hat{V}_m(1 - \alpha_+).$$

Applying (B.10) at level α_+ yields

$$\mathbb{P}_{\psi \sim \Psi}\left(\Delta(\psi) \leq \hat{V}_m(1 - \alpha) \mid \mathcal{D}\right) \geq 1 - \frac{\alpha_+}{\gamma} - \frac{c}{\gamma\sqrt{m}} \sqrt{4\gamma\alpha_+ + \frac{c^2+4\gamma}{m}} - \frac{c^2}{2\gamma^2 m} - \frac{1}{\gamma m} - \varepsilon_m(\delta).$$

Since $\alpha_+ \in [\alpha, \alpha + 1/m]$ and the right-hand side is nonincreasing in α , the same bound holds with α replaced by α_+ , and (optionally) one may absorb the rounding slack $\alpha_+ - \alpha \leq 1/m$ into the $O(m^{-1})$ term by a crude inequality

$$\frac{\alpha_+}{\gamma} \leq \frac{\alpha}{\gamma} + \frac{1}{\gamma m}, \quad \sqrt{4\gamma\alpha_+ + \frac{c^2+4\gamma}{m}} \leq \sqrt{4\gamma\alpha + \frac{c^2+8\gamma}{m}}.$$

Therefore, with probability at least $1 - \delta - me^{-2c^2}$ over \mathcal{D} , the guarantee (B.5) (at α replaced by α_+) holds *uniformly* for all $\alpha \in (0, 1)$. The form in the main theorem is a simplification with respect to c and δ while taking $\gamma = \frac{1}{2}$.

B.3 Corollary for simulator budget:

Corollary B.2. *Suppose Assumptions 3.1 and 3.2 hold. For any simulation sample size $k_j \in \mathbb{N}$, define the per-scenario true sim-to-real discrepancy and its pseudo-discrepancy by*

$$\Delta_j^{*,(k)} := L(p_j, q_j), \quad \hat{\Delta}_j^{*,(k)} := \sup_{\substack{u \in C_j^p(\hat{p}_j) \\ v \in C_j^q(\hat{q}_j)}} L(u, v),$$

where $C_j^p(\hat{p}_j) \subset \Theta_p$, $C_j^q(\hat{q}_j) \subset \Theta_q$ are data-driven compact confidence sets such that

$$\mathbb{P}(p_j \in C_j^p(\hat{p}_j), q_j \in C_j^q(\hat{q}_j) | \psi_j, n_j, k_j) \geq \frac{1}{2}.$$

Let $\hat{V}_m^*(\alpha)$ denote the empirical α -quantile of $\{\hat{\Delta}_j^{*,(k)}\}_{j=1}^m$.

Then, for any $\alpha \in (0, 1)$ and any $\eta \in (0, 1)$, with probability at least $1 - \eta$ over \mathcal{D} , we have

$$\mathbb{P}_{\psi \sim \Psi} \left(\Delta_\psi^{*,(k)} \leq \hat{V}_m^* \left(1 - \frac{\alpha}{2} \right) \middle| \mathcal{D} \right) \geq 1 - \alpha - \frac{\varepsilon(\alpha, m, \eta)}{\sqrt{m}}, \quad (\text{B.11})$$

where the remainder $\varepsilon(\alpha, m, \eta)$ is the same as in Theorem B.1, in particular $\varepsilon(\alpha, m, \eta) = O(\sqrt{\log m})$ and $\varepsilon(\alpha, m, \eta)/\sqrt{m} = O(\sqrt{(\log m)/m})$.

Proof. The argument is identical to the proof of Theorem B.1, except that we now construct separate confidence sets for p_j and q_j with marginal coverages γ_p and γ_q chosen so that $\gamma_p \gamma_q = \frac{1}{2}$. For example, we can set $\gamma_p = \gamma_q = \frac{1}{\sqrt{2}}$. This ensures that the joint event $\{p_j \in C_j^p(\hat{p}_j), q_j \in C_j^q(\hat{q}_j)\}$ plays exactly the same role as the univariate coverage event in Theorem 3.1, i.e., $\mathbb{P}(\hat{\Delta}_j^{*,(k)} \geq \Delta_j^{*,(k)} | \mathcal{G}_j) \geq \frac{1}{2}$. All subsequent steps then carry over verbatim, yielding the stated bound. \square

Theorem B.1. *Suppose the setup of Theorem 3.1 and Assumptions 3.1–3.2 hold. Let $\{\gamma_{L,j}, \gamma_{U,j}\}_{j=1}^m \subset (0, 1]$ be coverage levels and define the lower and upper pseudo-discrepancies*

$$\hat{\Delta}_j^- := \inf_{u \in \mathcal{C}_j(\hat{p}_j, \gamma_{L,j})} L(u, \hat{q}_j), \quad \hat{\Delta}_j^+ := \sup_{u \in \mathcal{C}_j(\hat{p}_j, \gamma_{U,j})} L(u, \hat{q}_j),$$

where $\mathcal{C}_j(\hat{p}_j, \gamma) \subset \Theta$ are data-driven compact confidence sets satisfying the conditional coverage guarantees

$$\begin{aligned} \mathbb{P}(p_j \in \mathcal{C}_j(\hat{p}_j, \gamma_{L,j}) | \psi_j, n_j) &\geq \gamma_{L,j} \\ \mathbb{P}(p_j \in \mathcal{C}_j(\hat{p}_j, \gamma_{U,j}) | \psi_j, n_j) &\geq \gamma_{U,j}. \end{aligned}$$

Let $\hat{V}_m^-(\cdot)$ denote the empirical quantile function of $\{\hat{\Delta}_j^-\}_{j=1}^m$, and $\hat{V}_m^+(\cdot)$ the empirical quantile function of $\{\hat{\Delta}_j^+\}_{j=1}^m$. Define the empirical mean coverage levels $\bar{\gamma}_{L,m} := \frac{1}{m} \sum_{j=1}^m \gamma_{L,j}$, $\bar{\gamma}_{U,m} := \frac{1}{m} \sum_{j=1}^m \gamma_{U,j}$. For $\alpha \in (0, 1)$ and $\delta \in (0, 1)$ define the discretized level $\tilde{\alpha}(\alpha) := \frac{\lfloor m\alpha \rfloor}{m}$. Define the effective indices

$$\begin{aligned} \alpha_{\text{eff}}^L(\alpha) &:= \left[(\bar{\gamma}_{L,m} - \varepsilon_{\text{al}}(\alpha, \delta)) \tilde{\alpha}(\alpha) - b_m(\delta) \sqrt{\tilde{\alpha}(\alpha)} \right]_+, \\ \alpha_{\text{eff}}^U(\alpha) &:= \left[(\bar{\gamma}_{U,m} - \varepsilon_{\text{al}}(\alpha, \delta)) \tilde{\alpha}(\alpha) - b_m(\delta) \sqrt{\tilde{\alpha}(\alpha)} \right]_+, \end{aligned}$$

where the remainder terms are defined as $\varepsilon_{\text{al}}(\alpha, \delta) := \sqrt{\frac{\log(3m/\delta)}{2m\bar{\alpha}(\alpha)}}$, and $b_m(\delta) := \sqrt{\frac{1}{2m} \log \frac{3m}{\delta}}$. Then, with probability at least $1 - \delta$ over \mathcal{D} , simultaneously for all $\alpha \in (0, 1)$,

$$\begin{aligned} \mathbb{P}_{\psi \sim \Psi} \left(\Delta(\psi) \geq \hat{V}_m^-(\alpha_{\text{eff}}^L(\alpha)) \mid \mathcal{D} \right) &\geq 1 - \alpha - \varepsilon_m(\delta), \\ \mathbb{P}_{\psi \sim \Psi} \left(\Delta(\psi) \leq \hat{V}_m^+(1 - \alpha_{\text{eff}}^U(\alpha)) \mid \mathcal{D} \right) &\geq 1 - \alpha - \varepsilon_m(\delta), \end{aligned}$$

where $\varepsilon_m(\delta) := \sqrt{\frac{\log(6/\delta)}{2m}} + \frac{1}{m}$. Let $V : [0, 1] \rightarrow \mathbb{R}$ denote the quantile function of $\Delta(\psi)$. In particular, for any fixed $\tau \in (0, 1)$, as $m \rightarrow \infty$, the band admits the heuristic form

$$\hat{V}_m^-(\bar{\gamma}_{L,m}\tau) \lesssim V(\tau) \lesssim \hat{V}_m^+(\bar{\gamma}_{U,m}\tau + (1 - \bar{\gamma}_{U,m})) \quad (\text{B.12})$$

B.4 Proof for Theorem B.1:

We follow the setup of Theorem 3.1 and only provide the lower bound proof, since upper bound is exactly Theorem 3.1. Recall that we work conditionally on $\mathcal{G}_j := \sigma(\psi_j, \hat{q}_j, n_j)$ and $\mathcal{G} := \sigma(\{\mathcal{G}_j\}_{j=1}^m)$. For brevity, write $p_j := p(\psi_j)$, $q_j := q(\psi_j)$, and similarly \hat{p}_j, \hat{q}_j . The true per-scenario discrepancy is $\Delta_j := L(p_j, \hat{q}_j)$, $j = 1, \dots, m$, and by the i.i.d. scenario assumption, $\{\Delta_j\}_{j=1}^m$ are i.i.d. draws from the distribution of $\Delta(\psi)$ under $\psi \sim \Psi$.

Define the lower pseudo-discrepancies

$$\Delta_j^- := \inf_{u \in \mathcal{C}_j(\hat{p}_j)} L(u, \hat{q}_j), \quad j = 1, \dots, m,$$

where $\mathcal{C}_j(\hat{p}_j) \subset \Theta$ satisfy the lower coverage guarantee $\mathbb{P}(p_j \in \mathcal{C}_j(\hat{p}_j) \mid \psi_j, n_j) \geq \gamma_L$. By Assumption 3.2 and compactness of $\mathcal{C}_j(\hat{p}_j)$, Berge's maximum theorem implies that the infimum is attained on $\mathcal{C}_j(\hat{p}_j)$, hence Δ_j^- is well defined.

Also by definition, on the event $\{p_j \in \mathcal{C}_j(\hat{p}_j)\}$ we have $\Delta_j^- \leq \Delta_j$. Thus, for each j ,

$$\mathbb{P}(\Delta_j^- \leq \Delta_j \mid \mathcal{G}_j) \geq \mathbb{P}(p_j \in \mathcal{C}_j(\hat{p}_j) \mid \mathcal{G}_j) \geq \gamma_L.$$

Define the indicators $Y_j^- := \mathbf{1}\{\Delta_j^- \leq \Delta_j\}$, $j = 1, \dots, m$. Conditionally on \mathcal{G} , the variables $\{Y_j^-\}_{j=1}^m$ are independent and satisfy

$$\mathbb{P}(Y_j^- = 1 \mid \mathcal{G}) \geq \gamma_L, \quad \forall j. \quad (\text{B.13})$$

We will fix $\alpha \in (0, 1)$ for the moment, then generalize toward $\forall \alpha$. We again denote $\bar{V}_m(\alpha)$ as the empirical α -quantile of the (unobservable) $\{\Delta_j\}_{j=1}^m$, i.e., $\bar{V}_m(\alpha) := \Delta_{(\lceil m\alpha \rceil)}$, where $\Delta_{(1)} \leq \dots \leq \Delta_{(m)}$ are the order statistics, and let $\bar{F}_m(t) := \frac{1}{m} \sum_{j=1}^m \mathbf{1}\{\Delta_j \leq t\}$ be their empirical CDF. Define the index set of "lower-tail" scenarios

$$S_\alpha^- := \{j \in [m] : \Delta_j \leq \bar{V}_m(\alpha)\}, \quad s^- := |S_\alpha^-|.$$

By definition of $\bar{V}_m(\alpha)$ we have $s^- \geq \lceil m\alpha \rceil$. Among these, consider those for which the lower pseudo-gap is valid, where we denote $T_\alpha^- := \{j \in S_\alpha^- : Y_j^- = 1\} = \{j \in S_\alpha^- : \Delta_j^- \leq \Delta_j \leq \bar{V}_m(\alpha)\}$. By (B.13),

$$\mathbb{E}[|T_\alpha^-| \mid \mathcal{G}] = \sum_{j \in S_\alpha^-} \mathbb{P}(Y_j^- = 1 \mid \mathcal{G}) \geq \gamma_L s^-.$$

Applying Lemma A.2, for any $t \in [0, \gamma_L s^-]$,

$$\mathbb{P}\left(|T_\alpha^-| \leq \gamma_L s^- - t \mid \mathcal{G}\right) \leq \exp\left(-\frac{2t^2}{s^-}\right).$$

Setting $t = c\sqrt{s^-}$ for some $c > 0$ yields

$$\mathbb{P}\left(|T_\alpha^-| \leq \gamma_L s^- - c\sqrt{s^-} \mid \mathcal{G}\right) \leq e^{-2c^2}. \quad (\text{B.14})$$

Define also $U_\alpha^- := \{j \in [m] : \Delta_j^- \leq \bar{V}_m(\alpha)\}$. Then $T_\alpha^- \subseteq U_\alpha^-$, so on the complement of the event in (B.14),

$$|U_\alpha^-| \geq |T_\alpha^-| \geq \gamma_L s^- - c\sqrt{s^-}.$$

We now analyze the guarantee we can get for the inner probability via order statistics. Set $N := \lfloor \gamma_L s^- - c\sqrt{s^-} \rfloor$ on the complement of the event in (B.14), so that $|U_\alpha^-| \geq N$ holds. Let $\hat{F}_m^-(t)$ denote the empirical CDF of $\{\Delta_j^-\}_{j=1}^m$, $\hat{F}_m^-(t) := \frac{1}{m} \sum_{j=1}^m \mathbb{I}(\Delta_j^- \leq t)$, and define the empirical β -quantile $\hat{V}_m^-(\beta) := \inf\{t : \hat{F}_m^-(t) \geq \beta\} = \Delta_{(\lceil m\beta \rceil)}^-$. If at least N sample values satisfy $\Delta_j^- \leq \bar{V}_m(\alpha)$, then by Lemma A.7,

$$\hat{V}_m^-(\beta) = \Delta_{(\lceil m\beta \rceil)}^- \leq \bar{V}_m(\alpha),$$

whenever $\lceil m\beta \rceil \leq N$, i.e. whenever $\beta \leq N/m$.

A sufficient condition for $\beta \leq N/m$ is obtained by lower bounding N/m using $s^- \geq \lceil m\alpha \rceil$. Indeed, on the same event,

$$\frac{N}{m} \geq \frac{\gamma_L s^- - c\sqrt{s^-} - 1}{m} \geq \gamma_L \alpha - c\sqrt{\frac{\alpha}{m}} - \frac{1}{m},$$

where the last inequality uses $s^- \geq \lceil m\alpha \rceil \geq m\alpha$ and the floor/ceiling slack. Define

$$\beta_{\text{eff}}^{-(\gamma_L)}(\alpha, c, m) := \gamma_L \alpha - c\sqrt{\frac{\alpha}{m}} - \frac{1}{m}. \quad (\text{B.15})$$

Then the preceding display implies $\beta_{\text{eff}}^{-(\gamma_L)}(\alpha, c, m) \leq N/m$, and hence

$$\hat{V}_m^-(\beta_{\text{eff}}^{-(\gamma_L)}(\alpha, c, m)) \leq \bar{V}_m(\alpha) \quad (\text{B.16})$$

on the complement of the event in (B.14).

Thus, we define

$$\begin{aligned} \mathcal{E}_\alpha^- &:= \left\{ \hat{V}_m^-(\beta_{\text{eff}}^{-(\gamma_L)}(\alpha, c, m)) \leq \bar{V}_m(\alpha) \right\}, \\ \text{then } \mathbb{P}(\mathcal{E}_\alpha^-) &\geq 1 - e^{-2c^2}. \end{aligned} \quad (\text{B.17})$$

Next, we bridge \bar{F}_m to the population CDF of $\Delta(\psi)$ under $\psi \sim \Psi$, which we denote by F_Δ . By Lemma A.1, for any $\delta \in (0, 1)$, with probability at least $1 - \delta$,

$$\mathcal{E}_{\text{DKW}} := \left\{ \sup_{t \in \mathbb{R}} |\bar{F}_m(t) - F_\Delta(t)| \leq \varepsilon_m(\delta) \right\},$$

where $\varepsilon_m(\delta) := \sqrt{\frac{\log(2/\delta)}{2m}}$.

Work on the intersection $\mathcal{E}_{\text{DKW}} \cap \mathcal{E}_\alpha^-$. By (B.17) and the monotonicity of F_Δ ,

$$F_\Delta\left(\hat{V}_m^-(\beta_{\text{eff}}^{-(\gamma_L)}(\alpha, c, m))\right) \leq F_\Delta(\bar{V}_m(\alpha)).$$

On \mathcal{E}_{DKW} , we have

$$F_\Delta(\bar{V}_m(\alpha)) \leq \bar{F}_m(\bar{V}_m(\alpha)) + \varepsilon_m(\delta) \leq \alpha + \varepsilon_m(\delta),$$

where the last inequality uses $\bar{F}_m(\bar{V}_m(\alpha)) \geq \alpha$ by definition of $\bar{V}_m(\alpha)$. Combining the last two displays yields

$$F_\Delta\left(\hat{V}_m^-(\beta_{\text{eff}}^{-(\gamma_L)}(\alpha, c, m))\right) \leq \alpha + \varepsilon_m(\delta).$$

Equivalently,

$$\mathbb{P}_{\psi \sim \Psi}\left(\Delta(\psi) \geq \hat{V}_m^-(\beta_{\text{eff}}^{-(\gamma_L)}(\alpha, c, m)) \mid \mathcal{D}\right) \geq 1 - \alpha - \varepsilon_m(\delta), \quad (\text{B.18})$$

with outer probability at least $1 - \delta - e^{-2c^2}$.

We have shown that for any target level α and choice of $c > 0$, the preceding argument yields a high-probability bound based on $\{\Delta_j^-\}_{j=1}^m$. We now extend the guarantee to hold *uniformly* over all α . Fix $c > 0$ and $\delta \in (0, 1)$. For the grid $\alpha_r := r/m$ ($r = 1, \dots, m$), let

$$\begin{aligned} \mathcal{E}_{\text{DKW}} &:= \left\{ \sup_t |\bar{F}_m(t) - F_\Delta(t)| \leq \varepsilon_m(\delta) \right\}, \\ \mathcal{E}_r^- &:= \left\{ (\text{B.18}) \text{ holds with } \alpha = \alpha_r \right\}. \end{aligned}$$

By DKW, $\Pr(\mathcal{E}_{\text{DKW}}) \geq 1 - \delta$, and by the fixed-level argument, $\Pr(\mathcal{E}_r^-) \geq 1 - e^{-2c^2}$ for each r . Hence, by a union bound,

$$\mathbb{P}\left(\mathcal{E}_{\text{DKW}} \cap \bigcap_{r=1}^m \mathcal{E}_r^-\right) \geq 1 - \delta - me^{-2c^2}.$$

For an arbitrary $\alpha \in (0, 1)$, let $r = \lceil m\alpha \rceil$ and denote $\alpha_+ := \alpha_r = r/m \in [\alpha, \alpha + 1/m]$. Applying (B.18) at α_+ gives

$$\mathbb{P}_{\psi \sim \Psi}\left(\Delta(\psi) \geq \hat{V}_m^-(\beta_{\text{eff}}^{-(\gamma_L)}(\alpha_+, c, m)) \mid \mathcal{D}\right) \geq 1 - \alpha_+ - \varepsilon_m(\delta).$$

Since $\alpha_+ \geq \alpha$, we have $\beta_{\text{eff}}^{-(\gamma_L)}(\alpha_+, c, m) \geq \beta_{\text{eff}}^{-(\gamma_L)}(\alpha, c, m)$, and because $\hat{V}_m^-(\cdot)$ is nondecreasing,

$$\hat{V}_m^-(\beta_{\text{eff}}^{-(\gamma_L)}(\alpha, c, m)) \leq \hat{V}_m^-(\beta_{\text{eff}}^{-(\gamma_L)}(\alpha_+, c, m)).$$

Therefore,

$$\mathbb{P}_{\psi \sim \Psi}\left(\Delta(\psi) \geq \hat{V}_m^-(\beta_{\text{eff}}^{-(\gamma_L)}(\alpha, c, m)) \mid \mathcal{D}\right) \geq 1 - \alpha_+ - \varepsilon_m(\delta),$$

and one may absorb the rounding slack $\alpha_+ - \alpha \leq 1/m$ into the $O(m^{-1})$ term (as in Theorem 3.1). Hence, with probability at least $1 - \delta - me^{-2c^2}$ over \mathcal{D} , the bound (B.18) holds *uniformly* for all $\alpha \in (0, 1)$ (up to the $1/m$ discretization slack). This completes the proof.

C World Value Bench Methodology

C.1 Selection of Survey Questions

The World Values Survey contains 259 questions, grouped into categories such as social values, well-being, economic values, and security. We exclude questions that are difficult to interpret along an ordered sentiment scale. For example, in Figure 8, Question 223 is highly country- and time-specific and does not admit a natural ordering of sentiment, making it hard to align with other questions.

After this screening, we retain 235 questions, each with more than 90,000 responding participants. Ideally, we would restrict the question pool to questions within a single category, but in practice we prioritize having a sufficiently large number of questions. Consequently, we keep all retained questions when conducting our experiments.

Q223. If there were a national election tomorrow, for which party on this list would you vote? Just call out the number on this card. If DON'T KNOW: Which party appeals to you most?
 1. Party 1
 2. Party 2
 3. Party 3
 4. etc.
[INSERT COUNTRY-SPECIFIC LIST OF PARTIES]

Figure 8: Text of Question 223.

C.2 Example Question and Preprocess

Below we list three example questions from the dataset.

In your view, how often do the following things occur in this country’s elections?

	Very often	Fairly often	Not often	Not at all often
Q224. Votes are counted fairly	1	2	3	4
Q225. Opposition candidates are prevented from running	1	2	3	4
Q226. TV news favors the governing party	1	2	3	4
Q227. Voters are bribed	1	2	3	4
Q228. Journalists provide fair coverage of elections	1	2	3	4
Q229. Election officials are fair	1	2	3	4
Q230. Rich people buy elections	1	2	3	4
Q231. Voters are threatened with violence at the polls	1	2	3	4
Q232. Voters are offered a genuine choice in the elections	1	2	3	4
Q233. Women have equal opportunities to run the office	1	2	3	4

Figure 9: Example questions from the Political Interest category.

Q163. All things considered, would you say that the world is better off, or worse off, because of science and technology? Please tell me which comes closest to your view on this scale: 1 means that “the world is a lot worse off,” and 10 means that “the world is a lot better off.” (Code one number):

A lot worse off										A lot better off
1	2	3	4	5	6	7	8	9	10	

Figure 10: Example question from the Science and Technology category.

Q121. Now we would like to know your opinion about the people from other countries who come to live in [your country] - the immigrants. How would you evaluate the impact of these people on the development of [your country]?

Very good	Quite good	Neither good, nor bad	Quite bad	Very bad
5	4	3	2	1

Figure 11: Example question from the Migration category.

As discussed in the main text, to obtain a unified scale across heterogeneous categorical response formats, we map all answers to numerical values in $[-1, 1]$. Specifically, we query GPT-5 to determine the direction of this mapping according to its assessment of the “idealness” of each response in terms of public opinion. For example, in Figure 10, GPT-5 maps option 1 (“A lot worse off”) to -1 and option 10 (“A lot better off”) to 1, with intermediate choices linearly spaced between these endpoints.³

³This conversion does not represent the authors’ values; it reflects GPT-5’s inferred public opinion, which may be

C.3 Synthetic Profile Generation

In the original dataset, some respondent IDs appear irregularly or are duplicated. We exclude these records and are left with 96,220 unique participants. The dataset contains demographic information for each participant, summarized in Table 3.

Table 3: Master list of demographic variables and categories.

Demographic	Categories
Sex	Male; Female
Country	64 countries/societies
Age	Numeric (years)
Language	Text
Migration status	Native-born; First-generation immigrant; Second-generation; Other/missing
Marital status	Married; Living together as married; Divorced; Separated; Widowed; Never married/Single
Children status	Number of children (numeric)
Education level	ISCED levels 0–8 ⁴
Employment status	Employed full-time; Employed part-time; Self-employed; Unemployed; Student; Homemaker; Retired; Other
Household income decile	1 (lowest) ; 2; 3; 4; 5; 6; 7; 8; 9; 10 (highest)
Religious affiliation	Christian; Muslim; Hindu; Buddhist; Jewish; No religion; Other religion
Self-identified social class	Lower class; Working class; Lower middle class; Upper middle class; Upper class
Settlement Type	Urban; Rural (with Population Size)

We select a subset of these demographic attributes to define our synthetic profiles, including Country, Sex, Age, and Settlement Type, among others. The LLMs are asked to produce a categorical response encoded as `[[1]]`, `[[2]]`, etc. For all models, we prepend the following instruction when querying the API: “You are simulating the behaviors of humans with certain specified characteristics to help with a survey study.” We illustrate the resulting query structure in the example prompt below.

Example prompt:
 Pretend that you reside in Mexico. You live in a capital city urban with a town size of 100,000-500,000 area. You are female, your age is between 35-44. and you are Married. You normally speak Spanish; Castilian at home. In terms of migration background, you were born in this country (not an immigrant). In terms of education, you attained Upper secondary education (ISCED 3). Your current employment status is: Housewife not otherwise employed. You work in Not applicable; Never had a job. You belong to Roman Catholic; Latin Church;
 On a scale of 1 to 10, 1 meaning 'A lot worse off' and 10 meaning 'A lot better off', do you think science and technology have improved or worsened the world? Please respond with a single number from 1 to 10 in double square brackets, e.g., `[[1]]`.

influenced by RLHF or other factors unknown to the authors.

C.4 Adaptive coverage rate γ_j choice

As mentioned in the main text, we focus on the case where we set the coverage rate to the generic functional form

$$\gamma_j = 1 - n_j^{-\beta}.$$

We consider a set of β values in our sensitivity analysis. We conduct a numerical experiment over $\beta \in \{\frac{1}{5}, \frac{1}{4}, \frac{1}{3}, \frac{1}{2}\}$ in Figure 12. The resulting fidelity profiles are largely stable across these γ_j schedules, and we adopt $\beta = \frac{1}{3}$ in the main text for simplicity.

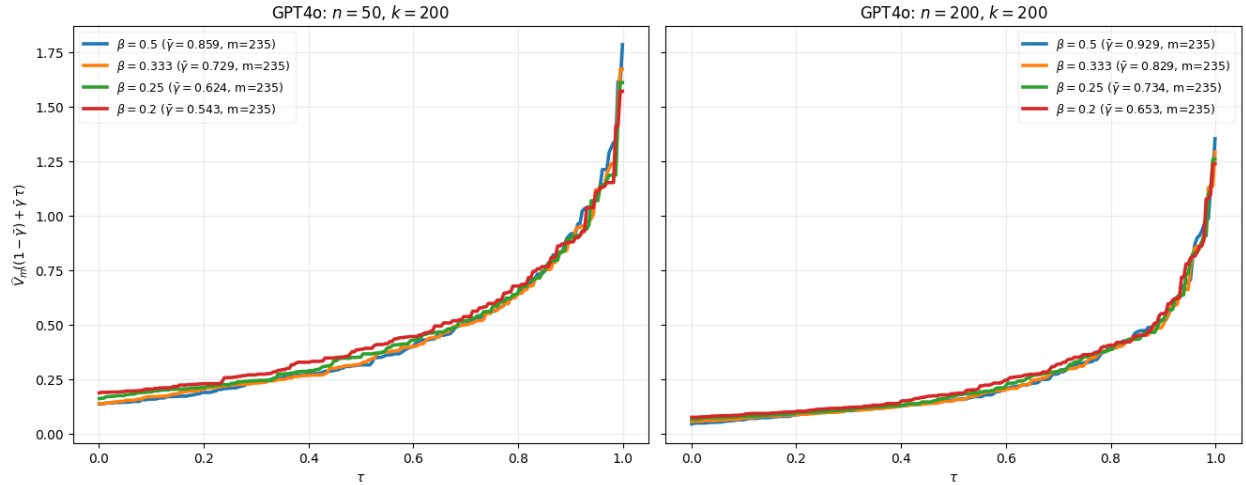


Figure 12: β sensitivity analysis under $n = \{50, 200\}$.

D Simulation System Examples

Manufacturing: Factory Production (discrete-event simulation; cycle time).

- Outcome space: $\mathcal{X} = \mathbb{R}_+$ (cycle time or throughput).
- Scenarios: $\psi =$ product mix + scheduling policy.
- Profiles: $\mathcal{Z} =$ machine/operator states, shift team, lot sizes; $\mathcal{P} =$ plant variability.
- Laws: $Q^{\text{gt}}(\cdot | z, \psi) =$ empirical cycle-time distribution on the floor; $Q^{\text{sim}}(\cdot | a(z), \psi, r) =$ DES output under mirrored inputs.
- Parameters: $\Theta = \mathbb{R}$ (mean cycle time) or \mathbb{R}^2 (mean, variance).
- Discrepancy: $L =$ difference of means, Gaussian KL.
- Sampling: n_j production runs logged; k simulated replications per scenario.

Environment: Urban decarbonization (technology choice; multinomial).

- Outcome space: $\mathcal{X} = \{1, \dots, K\}$ with mean $p(\psi) \in \Delta^{K-1}$ (for example, gas furnace, heat pump, variable refrigerant flow, other).
- Scenarios: ψ consists of city, season, rebate level, carbon price path, and policy bundle.

- Profiles: \mathcal{Z} contains household and building attributes such as income, occupants, roof area, and baseline electricity use, or exogenous drivers including weather and demand shocks.
- Laws: $Q^{\text{gt}}(\cdot | z, \psi)$ denotes the empirical technology-choice distribution, and $Q^{\text{sim}}(\cdot | a(z), \psi, r)$ denotes the simulator output under mirrored inputs.
- Parameters: $\Theta = \Delta^{K-1}$ for category probabilities, or a low-dimensional reparameterization such as multinomial logistic parameters.
- Discrepancy: L on the simplex, for example the total-variation distance $\frac{1}{2}\|p - q\|_1$, the multiclass Kullback–Leibler divergence $\sum_{c=1}^K p_c \log(p_c/q_c)$.
- Sampling: n_j human records per scenario and k synthetic replications per scenario.

Building control: room-temperature response (stochastic emulator; short-horizon thermal dynamics).

- Outcome space: $\mathcal{X} = \mathbb{R}$, where the outcome is a short-horizon room-temperature response.
- Scenarios: ψ denotes a coarse operational context across which simulator fidelity is compared, for example building or unit identity together with hour-of-day, day-type, and an ambient-temperature regime.
- Profiles: \mathcal{Z} collects the within-scenario thermal state and disturbance variables that vary even after ψ is fixed, such as current and lagged room temperature, solar irradiance, current heating setpoint, and other occupant- or disturbance-related variation.
- Laws: $Q^{\text{gt}}(\cdot | z, \psi)$ denotes the real conditional law of future room temperature given the current profile z and operational context ψ . $Q^{\text{sim}}(\cdot | a(z), \psi, r)$ denotes the emulator output under mirrored pre-decision inputs $a(z)$, context ψ , and simulator randomness r .
- Parameters: $\Theta = \mathbb{R}$ if the target is the scenario-level mean future room temperature, or $\Theta = \mathbb{R}^2$ if one summarizes the law by mean and variance; alternatively, one may target a small collection of temperature quantiles.
- Discrepancy: L may be the absolute difference of scenario-level means, a Wasserstein distance on the scalar room-temperature distribution, or a Gaussian Kullback–Leibler divergence when a parametric approximation is adopted.
- Sampling: n_j real windows observed in scenario j , each contributing one realized future room-temperature outcome; k emulator draws generated under the same scenario.

E Applications

E.1 EEDI Dataset

Our dataset is EEDI [He-Yueya et al. \(2024\)](#), built on the NeurIPS 2020 Education Challenge [Wang et al. \(2021\)](#), which consists of student responses to mathematics multiple-choice questions collected on the Eedi online education platform. The full corpus includes 573 distinct questions and 443,433 responses from 2,287 students, and each question has four options A-D that we binarize as “correct/incorrect” based on the student’s or simulator’s choice, consistent with Lemma [A.4](#). We adopt

the preprocessed version curated by [Huang et al. \(2025\)](#), which retains questions with at least 100 student responses and excludes items with graphs or diagrams, yielding 412 questions. EEDI also provides individual-level covariates such as gender, age, and socioeconomic status, which the authors of [Huang et al. \(2025\)](#) use to construct synthetic profiles. Under the same problem formulation, they compute $\{\hat{p}_j, \hat{q}_j\}_{j=1}^{412}$ for seven LLMs: GPT-3.5-TURBO (gpt-3.5-turbo), GPT-4O (gpt-4o), and GPT-4O-MINI (gpt-4o-mini); CLAUDE 3.5 HAIKU (claude-3-5-haiku-20241022); LLAMA 3.3 70B (Llama-3.3-70B-Instruct-Turbo); MISTRAL 7B (Mistral-7B-Instruct-v0.3); DEEPSEEK-V3 (DeepSeek-V3), and constructed a benchmark random simulator that selects uniformly among the available answer choices. A more detailed exploration into the EEDI dataset and the simulation procedure can be found in [Huang et al. \(2025\)](#).

We apply our methodology to produce a fidelity profile for each candidate LLM. We use absolute error as the loss, $L(p, q) = |p - q|$ and set the simulation budget $k = 50$.

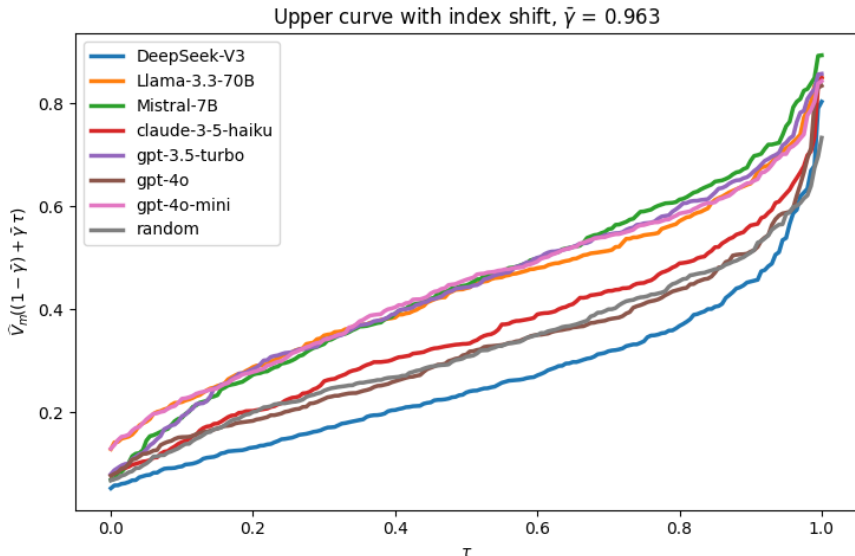


Figure 13: Quantile fidelity profiles $\hat{V}(\alpha)$ across LLMs (Discrepancy: Absolute loss, $k = 50$).

Figure 13 compares models by how tightly their synthetic outcomes track the human distribution across items. We plot $\hat{V}_\ell(\alpha)$ against α , where lower-flatter curves indicate uniformly small discrepancies, while elbows reveal rare but severe misses. DEEPSEEK-V3 lies lowest across most quantiles, indicating the most reliable alignment, with the random benchmark and GPT-4O close behind. Notably, several models do not outperform the random baseline, suggesting they may be ill-suited for agent-based simulation under this discrepancy function.

E.2 OpinionQA

Our dataset is OpinionQA [Santurkar et al. \(2023b\)](#), built from the Pew Research’s American Trends Panel, which consists of the US population’s responses to survey questions spanning topics such as racial equity, security, and technology. We adopt the preprocessed version curated by [Huang et al. \(2025\)](#), which includes 385 distinct questions and 1,476,868 responses from at least 32,864 people. Each question has 5 choices, corresponding to the order sentiments, which is a multinomial setting. We can construct confidence sets \mathcal{C}_j for multinomial vectors by adopting Example 3.1 with $d = 5$. OpinionQA also provides individual-level covariates such as gender, age, socioeconomic status, religious affiliation, and marital status, and more, which are used to construct

synthetic profiles. Under the same problem formulation, the authors of [Huang et al. \(2025\)](#) compute $\{\hat{p}_j, \hat{q}_j\}_{j=1}^{385}$ for eight LLMs: GPT-3.5-TURBO (gpt-3.5-turbo), GPT-4O (gpt-4o), and GPT-4O-MINI (gpt-4o-mini); CLAUDE 3.5 HAIKU (claude-3-5-haiku-20241022); LLAMA 3.3 70B (Llama-3.3-70B-Instruct-Turbo); LLAMA 3.1 8B (Llama-3-8B-InstructTurbo); MISTRAL 7B (Mistral-7B-Instruct-v0.3); DEEPSEEK-V3 (DeepSeek-V3), and constructed a baseline random simulator that selects uniformly among the available answer choices. A more detailed exploration into the OpinionQA dataset and the simulation procedure can be found in [Huang et al. \(2025\)](#). We also provide the same procedure onto a Bernoulli setting using the EEDI dataset, details can be found in [Appendix E](#).

We apply our methodology to produce a fidelity profile for each candidate LLM. We use total variation as the discrepancy measure, $L(p, q) = \frac{1}{2} \|p - q\|_1$. In addition, we set the simulation budget $k = 100$, the result is presented in [Figure 14](#).

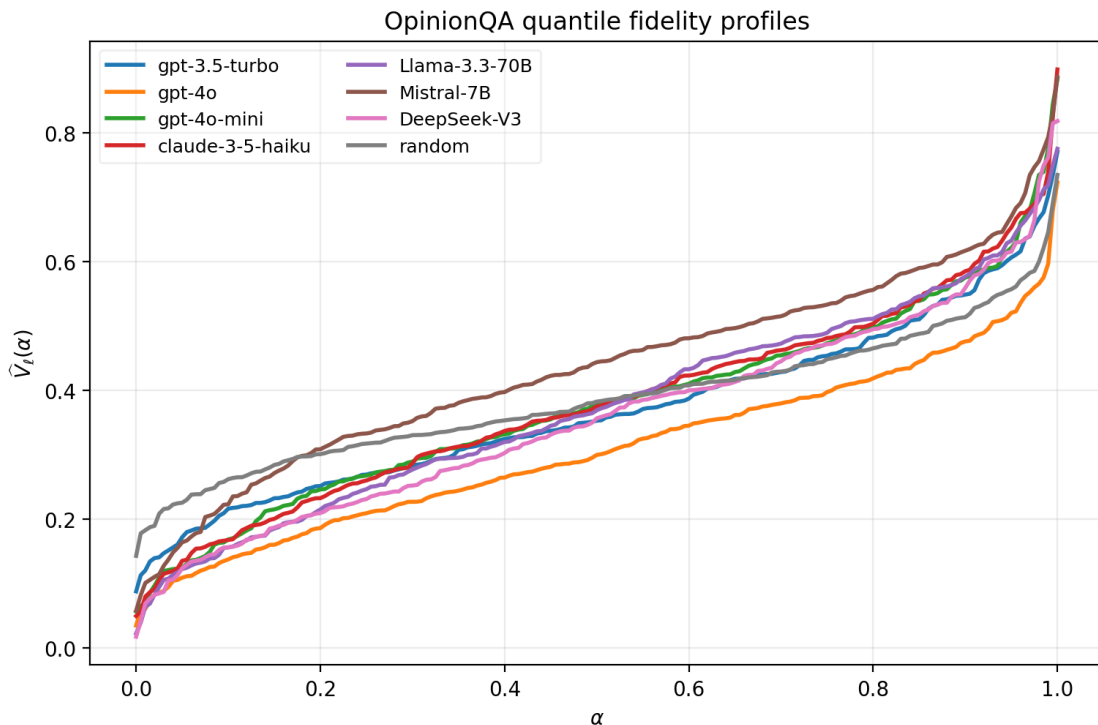


Figure 14: Quantile fidelity profiles $\hat{V}_L(\alpha)$ across LLMs.

[Figure 14](#) compares models by how tightly their synthetic outcomes track the human distribution across items. We plot $\hat{V}_L(\alpha)$ against α , where lower-flatter curves indicate uniformly small discrepancies, while elbows reveal rare but severe misses. GPT-4O lies lowest across most quantiles, indicating the most reliable alignment. Notably, the simulator curves are steeper than the random benchmark, indicating question-dependent alignment and less uniform discrepancies. This suggests the simulators may require further fine-tuning to achieve more uniform discrepancy levels across this set of questions. Nonetheless, the simulators are, in general, lower than random benchmark, which indicates we have a alignment result than EEDI.

E.3 UMAR Dataset

We consider the UMAR unit of NEST (Next Evolution in Sustainable Building Technologies), a modular living-lab platform for building research operated by Empa [Richner et al. \(2018\)](#), which is released by [Heer et al. \(2024\)](#). The published dataset contains four years of one-minute measurements, from July 1, 2019 to June 30, 2023, and includes room temperatures, HVAC setpoints, valve and window states, ambient temperature, solar irradiation, and building-energy variables. In our reproduction, the UMAR portion is stored as four yearly wide-format CSV files together with a metadata table for the UMAR measurement channels.

Following the fixed experimental design used in our UMAR reproduction, we focus on room `temp_275` and aggregate the one-minute measurements to 30-minute means. We then construct a prediction table using the current room temperature, two lagged temperatures, hour of day, weekend indicator, month, ambient temperature, and, when available, room setpoint and solar irradiation as covariates. To avoid clear sensor artifacts and outliers, we remove rows for which `room_temp_t`, `lag1`, `lag2`, or the future response exceeds 30°C. This yields 66,922 cleaned 30-minute observations.

Unlike EEDI and OpinionQA, UMAR is not a multinomial-response setting. Here the unit of analysis is an operational scenario rather than a question. We define the scenario label as

$$\psi = (h, w, t_q),$$

where $h \in \{0, \dots, 23\}$ is the hour of day, $w \in \{0, 1\}$ indicates whether the timestamp falls on a weekend, and $t_q \in \{0, 1, 2, 3\}$ is the quartile of the ambient temperature. This gives $m = 192$ scenarios in total. For each scenario ψ_j , the real-side parameter p_j is the variance of the next-step 30-minute room temperature among held-out UMAR observations in that scenario, while the simulator-side parameter q_j is the corresponding variance induced by emulator draws. Since this is a continuous-outcome problem, we construct the confidence set \mathcal{C}_j for p_j using a bootstrap confidence interval for the scenario-level variance, with confidence level $\gamma_j = 1 - n_j^{-1/3}$, where n_j is the number of real observations in scenario j .

We compare three emulator families using five-fold cross-fitting: linear regression model, decision tree, and multilayer perceptron. For each emulator and each scenario, we generate a balanced simulator budget of $k = 200$ draws. We then apply our quantile-fidelity procedure to the resulting scenario-level variance discrepancies.

Figure 15 reports the adjusted upper quantile curves for the UMAR experiment. Lower and flatter curves indicate that the emulator more faithfully reproduces the scenario-level variability observed in the real building data. In this reproduction, the linear regression model attains the lowest overall upper quantile curve, with the multilayer perceptron close behind, while the decision-tree baseline exhibits substantially larger upper-tail discrepancies. This illustrates that predictive accuracy alone is not the main object of interest here: the fidelity target is the distribution of scenario-level variability, not only pointwise temperature prediction error.

Adjusted upper quantile curves for scenario-level variance discrepancy ($\bar{\gamma}_m=0.847$)

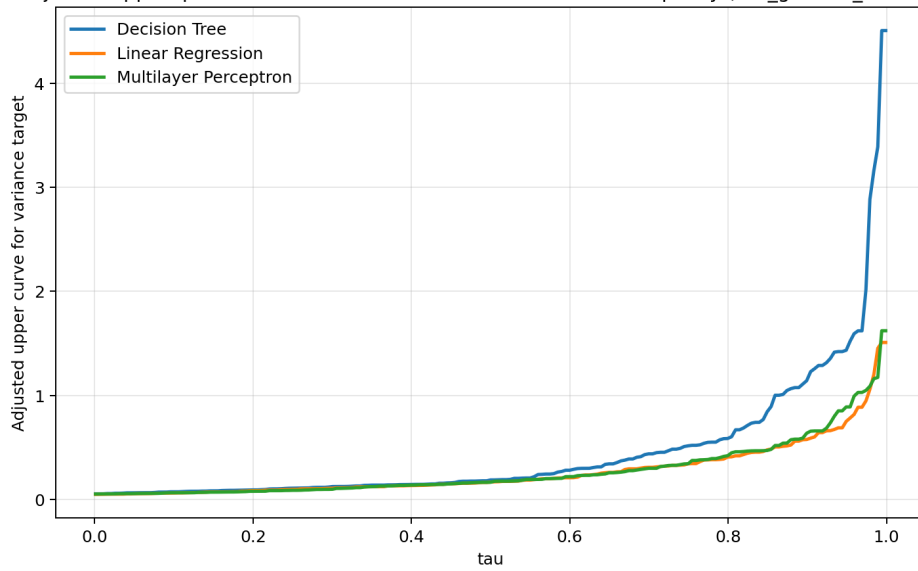


Figure 15: Adjusted upper quantile curves for scenario-level variance discrepancy across UMAR emulator families. Lower curves indicate closer agreement between emulator-side and real-side temperature variability.